Standard Title Page - Report on State Project

Report No.	Report Date	No. Pages	Type Report: Final	Project No.: 71179
VTRC 05-CR26	June 2005	64	Period Covered: 12/10/03 – 6/30/05	Contract No.

Title:
Characterization of the Punching Shear Capacity of Thin Ultra-High Performance Concrete Slabs

Key Words:
ultra-high performance concrete; fiber reinforced concrete; shear capacity; prestressed concrete

Authors:
D.K. Harris and C.L. Roberts-Wollmann

Performing Organization Name and Address:

Virginia Transportation Research Council
530 Edgemont Road
Charlottesville, VA 22903

Sponsoring Agencies' Name and Address

Virginia Department of Transportation
1401 E. Broad Street
Richmond, VA 23219

Supplementary Notes

Abstract

Ultra-high performance concrete (UHPC) is a relatively new type of concrete that exhibits mechanical properties that are far superior to those of conventional concrete and in some cases rival those of steel. The main characteristics that distinguish UHPC from conventional reinforced concrete are its very high compressive strength (20 to 33 ksi), the addition of steel fibers which enables tension to be carried across open cracks without conventional reinforcing steel, and a very high resistance to corrosion and degradation. The mechanical properties of UHPC allow for smaller, thinner sections as compared to conventional reinforced concrete sections. However, as it is a new material**,** the use of UHPC has been limited to a few structural applications due primarily to the high cost of the material and the lack of established design guidelines.

In previous research, a material model based on physical tests was used in conjunction with finite element models to develop an optimized cross-section for a prestressed UHPC girder for bridge applications. The cross-section is a double-tee with bulbs at the bottoms of the webs to accommodate the prestressing strands. As it is envisioned in bridge applications, the double-tees will be placed directly adjacent to one another, and the top flange will act as the riding surface after a thin asphalt overlay is placed. Based on the longitudinal compressive stresses, the top flange of the girder can be quite thin. However, there exists the possibility that a punching shear failure could occur from the application of a point load such as a wheel patch load if the flange is made too thin. The research reported herein was initiated to characterize the punching shear capacity of thin UHPC plates and to develop recommendations on the minimum top flange thickness for the optimized double-tee.

Twelve small slabs (45 in x 45 in) were tested to failure to characterize the punching shear strength of UHPC. The variables considered were the slab thickness (2, 2.5, and 3 in) and loading plate dimensions (from 1 in x 1 in to 3 in x 3 in). The results of the testing were compared to several existing models for punching shear. The two equations that predicted strengths most reliably were the current ACI punching shear equation and a modified bolt pull-out equation. After evaluation of the test results, the minimum slab thickness required to prevent a punching shear failure in the top flange due to an 8 in x 20 in wheel patch was determined to be 1 in.

Three larger slabs were also tested. These slabs had the same clear span length as the top flange of the optimized double-tee and were loaded with a wheel patch load. The slabs were all approximately 3 in thick and all failed in flexure rather than punching shear. It was concluded that the casting method has a strong influence on the orientation of the steel fibers, which in turn influences the flexural strength in orthogonal directions in the slab. The top flange thickness will be governed by transverse bending rather than punching shear, and the 3 in slabs were not able to support the full wheel load plus impact and load factor.

The results of this research help in the continued optimization of a UHPC shape for use in highway bridges. If material use in the girder is minimized, UHPC bridges can become economically competitive with HPC bridges, but offer the benefits of more rapid construction and better durability.

Copyright by the Virginia Center for Transportation Innovation and Research. D.K. Harris and C.L. Roberts-Wollmann. "Characterization of the Punching Shear Capacity of Thin Ultra-High Performance Concrete Slabs," Virginia Transportation Research Council 530 Edgemont Road Charlottesville, VA 22903, Report No. VTRC 05-CR26, June 2005.

FINAL CONTRACT REPORT

CHARACTERIZATION OF THE PUNCHING SHEAR CAPACITY OF THIN ULTRA-HIGH PERFORMANCE CONCRETE SLABS

D. K. Harris
Graduate Research Engineer

C. L. Roberts-Wollmann, Ph.D., P.E.
Assistant Professor

Via Department of Civil and Environmental Engineering
Virginia Polytechnic Institute & State University

Project Manager
Michael C. Brown, Ph.D., P.E. Virginia Transportation Research Council

Contract Research Sponsored by
Virginia Transportation Research Council

Virginia Transportation Research Council
(A Cooperative Organization Sponsored Jointly by the
Virginia Department of Transportation and
the University of Virginia)

Charlottesville, Virginia

June 2005
VTRC 05-CR26

NOTICE

The project that is the subject of this report was done under contract for the Virginia Department of Transportation, Virginia Transportation Research Council. The contents of this report reflect the views of the authors, who are responsible for the facts and the accuracy of the data presented herein. The contents do not necessarily reflect the official views or policies of the Virginia Department of Transportation, the Commonwealth Transportation Board, or the Federal Highway Administration. This report does not constitute a standard, specification, or regulation.

Each contract report is peer reviewed and accepted for publication by Research Council staff with expertise in related technical areas. Final editing and proofreading of the report are performed by the contractor.

Copyright 2005 by the Commonwealth of Virginia.

ABSTRACT

Ultra-high performance concrete (UHPC) is a relatively new type of concrete that exhibits mechanical properties that are far superior to those of conventional concrete and in some cases rival those of steel. The main characteristics that distinguish UHPC from conventional reinforced concrete are its very high compressive strength (20 to 33 ksi), the addition of steel fibers which enables tension to be carried across open cracks without conventional reinforcing steel, and a very high resistance to corrosion and degradation. The mechanical properties of UHPC allow for smaller, thinner sections as compared to conventional reinforced concrete sections. However, as it is a new material**,** the use of UHPC has been limited to a few structural applications due primarily to the high cost of the material and the lack of established design guidelines.

In previous research, a material model based on physical tests was used in conjunction with finite element models to develop an optimized cross-section for a prestressed UHPC girder for bridge applications. The cross-section is a double-tee with bulbs at the bottoms of the webs to accommodate the prestressing strands. As it is envisioned in bridge applications, the double-tees will be placed directly adjacent to one another, and the top flange will act as the riding surface after a thin asphalt overlay is placed. Based on the longitudinal compressive stresses, the top flange of the girder can be quite thin. However, there exists the possibility that a punching shear failure could occur from the application of a point load such as a wheel patch load if the flange is made too thin. The research reported herein was initiated to characterize the punching shear capacity of thin UHPC plates and to develop recommendations on the minimum top flange thickness for the optimized double-tee.

Twelve small slabs (45 in x 45 in) were tested to failure to characterize the punching shear strength of UHPC. The variables considered were the slab thickness (2, 2.5, and 3 in) and loading plate dimensions (from 1 in x 1 in to 3 in x 3 in). The results of the testing were compared to several existing models for punching shear. The two equations that predicted strengths most reliably were the current ACI punching shear equation and a modified bolt pull-out equation. After evaluation of the test results, the minimum slab thickness required to prevent a punching shear failure in the top flange due to an 8 in x 20 in wheel patch was determined to be 1 in.

Three larger slabs were also tested. These slabs had the same clear span length as the top flange of the optimized double-tee and were loaded with a wheel patch load. The slabs were all approximately 3 in thick and all failed in flexure rather than punching shear. It was concluded that the casting method has a strong influence on the orientation of the steel fibers, which in turn influences the flexural strength in orthogonal directions in the slab. The top flange thickness will be governed by transverse bending rather than punching shear, and the 3 in slabs were not able to support the full wheel load plus impact and load factor.

The results of this research help in the continued optimization of a UHPC shape for use in highway bridges. If material use in the girder is minimized, UHPC bridges can become economically competitive with HPC bridges, but offer the benefits of more rapid construction and better durability.

FINAL CONTRACT REPORT

CHARACTERIZATION OF PUNCHING SHEAR CAPACITY OF THIN UHPC SLABS

D. K. Harris
Graduate Research Engineer

C. L. Roberts-Wollmann, Ph.D., P.E.
Assistant Professor

Via Department of Civil and Environmental Engineering
Virginia Polytechnic Institute & State University

INTRODUCTION

Ultra-high performance concrete (UHPC) is a relatively new type of concrete that exhibits mechanical properties that are far superior to those of conventional concrete and in some cases rival those of steel. The compressive strength of UHPC has been reported to be between 20 and 33 ksi. Additionally, due to the addition of a large quantity of steel fibers, UHPC has the ability to carry tensile stresses across open cracks, unheard of in conventional concrete, which allows for the possibility of eliminating steel reinforcement in some applications. The use of UHPC allows for section dimensions to be minimized, taking advantage of the improved material properties and minimizing material usage and cost. In addition to the improved strength properties, UHPC has a very low permeability, making the material resistant to the corrosion and deterioration often associated with reinforced concrete and steel structures. This resistance directly correlates to a longer service life that can be achieved with the use of UHPC, making it an ideal material for a number of structural applications, particularly bridge structures.

The benefits of UHPC are quite substantial, but are offset by the high cost of the material. With the material being relatively new, there have only been a limited number of structural applications and the costs have remained high because the material is still considered to be a specialty product. The expectation is that as design with UHPC becomes a more common practice and shapes are optimized for the material properties, the costs will decrease as the industry becomes more familiar and comfortable with it.

Park et al. (2003) have developed a material model for UHPC and an optimized section for use as a bridge girder with an integrated riding surface. The model developed was validated with results from testing performed by the Federal Highway Administration (FHWA). The cross-section is a double-tee with bulbs at the bottom of the webs to accommodate the prestressing strands. As it is envisioned in bridge applications, the double-tees will be placed adjacent to one another, and the top flange will act as the riding surface after a thin topping is placed. The optimized section minimizes the material usage and eliminates the use of shear reinforcement. With all of the dimensions minimized, the resulting section has a thin top flange

that also serves as the riding surface. The possibility exists that a punching shear failure could occur with a tire patch load applied to the surface if the top flange is too thin.

PURPOSE AND SCOPE

This main objective of this study was to develop a model and recommend an equation for the prediction of the punching shear capacity of UHPC slabs. This work is being performed in support of the work done by the FHWA in the development and testing of the optimized double-tee section. The punching shear equation can assist in the determination of the smallest top flange thickness for the new bridge girder shape.

To accomplish this objective, two types of slab tests were performed. First, twelve 45 in by 45 in (36 in by 36 in unsupported area) slabs were tested to failure to determine punching shear capacity. The slabs were initially designed based on a modification of the ACI equation to calculate punching shear capacity and a yield line analysis to calculate flexural capacity. It was determined that to force a punching shear failure prior to a flexural failure, the slabs would have to be fixed against rotation on all edges and the punches would have to be quite small. Three slab thicknesses, 2 in, 2.5 in and 3 in were tested with varying loading plate areas. The results of the testing were then compared to several models for punching shear to develop recommendations as to the best predictor of punching shear strength of UHPC slabs.

The second type of slab modeled the actual conditions in the top flange of the optimized double-tee. The three slabs were 7 ft by 12 ft and approximately 3 in thick. Originally the slabs were to be 2 in, 2.5 in, and 3 in thick, however, due to casting errors, they were all approximately the same thickness. These slabs were supported along their long edges, and unsupported on the short edges. The clear span of the slab was approximately the same as the clear span between web walls on the double-tee. The slabs were loaded through a wheel patch load to determine if they were able to support a design wheel load, and to determine the failure mechanism. The results of these tests are also used to develop recommendations for the top flange thickness of the optimized double-tee.

METHODS AND MATERIALS

Ultra-High Performance Concrete

Limited research has been conducted on the mechanical properties of UHPC, with none specifically devoted to the punching shear capacity of UHPC slabs. The following section discusses the history, properties, and capabilities of UHPC. In addition, a brief summary of the modeling optimization study for UHPC conducted at MIT is provided, as it serves as a cornerstone of this research effort.

History of UHPC

UHPC is a relatively new type of concrete that provides significant improvements in strength, ductility, workability, and durability when compared to reinforced concrete or conventional high-performance concrete (HPC). The distinguishing factor between UHPC and HPC is that these improved characteristics are inherent to UHPC, whereas with HPC the mix is designed to meet special combinations of performance and uniformity requirements (Semioli 2001).

The recent development of UHPC has been primarily spearheaded by two independent French constructors, Bouygues Construction and Eiffage Group (EGI), with the aid of construction materials companies, Lafarge Corporation and Sika Corporation, respectively. The independent efforts of both companies created the products, Ductal®, brand name for Bouygues and BSI (Béton Special Industriel), brand name for EGI, with similar characteristics. While both materials exhibit similar qualities, the focus of this research effort is centered on Ductal® , which was the material used in all specimens.

General Composition

UHPC, specifically Ductal®, contains many of the same constituent materials as conventional concrete mix designs, but the proportions are quite different (Graybeal and Hartmann 2003). The UHPC composition provided in Table 1 is derived from testing conducted by Graybeal and Hartmann (2003) and is used primarily for comparative purposes.

Table 1 - Comparison of UHPC Composition to HPC

Material	UHPC Amount (lb/yd^3)	10,000 psi HPC* Amount (lb/yd^3)
Portland Cement	1200	752
Coarse Aggregate	0	1671
Fine Sand	1720	1350
Silica Fume	390	75
Ground Quartz	355	0
Super Plasticizer	51.8	0
Steel Fibers	263	0
Accelerator	50.5	0
Water Reducer	0	207 fl oz.
Air Entrainment	0	6.6 fl oz.
Retarder	0	25-30 fl oz.
Water	184	235

**Mix design from Virginia Avenue Bridge over Clinch River-Richlands, VA (TFHRC 2004)*

The most distinguishing characteristics of the composition of UHPC are the lack of coarse aggregate, the use of steel fibers, high proportion of cement/cementitious materials, and low volume of water. The use of only fine sand aggregate minimizes imperfections in the aggregates and creates a dense concrete matrix with minimal voids, which results in a significant increase in strength. The steel fibers in the concrete matrix are designed to provide a bond at the micro level and minimize micro-cracking (Figure 1). In turn they act as micro-reinforcement similar to mild steel reinforcement in conventional reinforced concrete on the macro level (Perry 2003a).

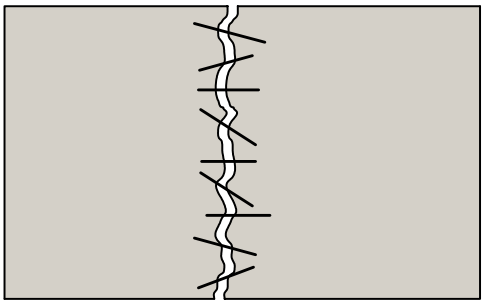

Figure 1. Representation of Fiber Contribution

Material Physical Properties

The majority of the improvements in material properties can be attributed to the finely graded and tightly packed materials and steel fibers that aid in holding the cement matrix together after cracking has occurred (Graybeal and Hartmann 2003).

Compressive Strength and Modulus

One of the most significant assets of UHPC is the very high compressive strength; UHPC has been demonstrated to achieve compressive strengths ranging from 23-33 ksi depending on the heat treatment (Perry and Zakariasen 2003). This compressive strength is significantly higher than conventional concretes and may allow for the possibility of UHPC to be competitive in markets that have been typically dominated by steel construction.

In tests conducted by Graybeal and Hartmann (2003) at the FHWA laboratory, the curing method used resulted in significant variations in compressive strength, up to a 65% difference between steam curing and ambient air curing. While various curing methods can be specified in field applications, the quality control required for these curing methods makes UHPC more suitable for precast operations.

Modulus of elasticity values have been reported to be between 8000 and 9000 ksi (Ahlborn et al. 2003).

Tensile Strength / Flexural Strength

The high compressive strength of UHPC is complemented by the fact that it also exhibits tensile strength that has not been demonstrated in conventional concretes. This tensile strength allows the material to support both pre-cracking and post-cracking loads without experiencing the brittle failure that would be common in a conventional concrete. UHPC has demonstrated tensile strengths ranging from 0.9-1.7 ksi with various curing regimes and standard ASTM testing methods (Graybeal and Hartmann 2003). These tensile strengths were achieved as a result of the interaction of the steel fibers on the microscopic level and their ability to sustain load after the onset of cracking.

In addition to the high tensile strength, UHPC can also achieve flexural strengths ranging from 5.0–7.2 ksi based on standard flexural beam tests (Perry and Zakariasen 2003). Beam tests have shown that UHPC is capable of supporting significant loads beyond cracking. This combination of the unique physical properties of UHPC allows designers to create thinner sections, longer spans, and taller structures (Perry and Zakariasen 2003).

Other Physical Properties

In addition to improved strength and ductility, UHPC exhibits some characteristics that make it very attractive for use in a number of applications. Due to the dense cementitious matrix and small and disconnected pore structure, UHPC maintains a very low permeability: roughly 1/10 that of granite (Lafarge 2004). UHPC allows for negligible carbonation or penetration of chlorides/sulfates and also maintains a high resistance to acid attack (Perry and Zakariasen 2003). UHPC's excellent resistance to freeze-thaw cycles also develops from the dense matrix, making it ideal for virtually any climate condition.

UHPC also exhibits very low creep and shrinkage after heat treatment when compared to conventional concretes, making the material suitable for precast/prestressed structures (Perry and Zakariasen 2003). The material can also be classified as a self-forming (self-consolidating) concrete due to the ease of flow of the material, which can be poured or pumped into place with limited or no vibration.

Advantages

With the significantly improved physical properties of UHPC, there are a number of advantages when compared to conventional concretes and even steel for structural applications. The high strength of UHPC allows the designer to use smaller sections, requiring less material to yield the same load carrying capacity. The properties of UHPC can be optimized when used in conjunction with prestressing, which maximizes the use of the inherent tensile capabilities. The presence of the steel fiber reinforcement and interaction of the matrix allow for the elimination of flexural and shear mild reinforcement in a number of cases.

Due to the durability and low permeability, UHPC structures are expected to have a longer service life than conventional reinforced concrete structures. UHPC is designed to be able to resist the effects of damaging environments and save money over the life of a project.

Disadvantages

The biggest disadvantage of using UHPC in today's market is the initial cost. It also has a very long mix time and requires high-energy mixers to properly mix. With UHPC being relatively new to the industry, there have been only a limited number of applications. The design and use of the material has not yet been optimized or streamlined and as a result, the cost is still significantly higher than that of conventional concrete. The producers expect that as UHPC becomes more commonly used in practice, the cost will decrease and they suggest that savings will be achieved over the life cycle when compared to conventional solutions.

While the strength of UHPC allows for minimization of section properties, design with UHPC must still meet the stiffness requirements for serviceability. There is a limit as to how thin or small a member can be and still satisfy deflection and vibration criteria.

Another difficulty with the use of UHPC in design is that it is more suited for use in a precasting facility rather than onsite applications. UHPC in standard bridge girder shapes does not allow for use of the material to its full potential; however, standard sections can be minimized (shorter sections, thinner flanges/webs, etc.) to make better use of the material properties. Also, formwork must be carefully designed and curing carefully monitored, because UHPC exhibits considerable early age shrinkage. The formwork must be designed so it can be released to allow the UHPC concrete to shrink without restraint.

Model-Based Optimization of UHPC

UHPC Model and Model Validation

Park et al. (2003) concluded that UHPC can be characterized as a material with two phases, the high strength cementitious matrix and the high strength fiber reinforcement, with distinct kinematics and possible mechanical interaction. UHPC is capable of supporting load until the point of cracking of the cementitious matrix and then can continue to support additional load after a minimal drop in stress (Figure 2).

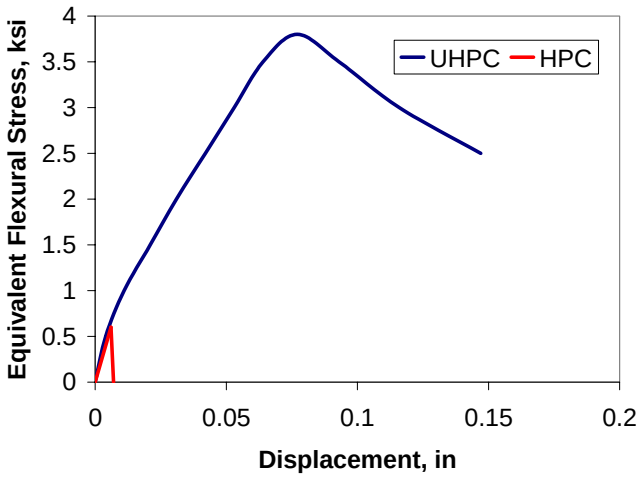

Figure 2. Equivalent Flexural Stress vs. Deflection of Ductal® and Conventional HPC

A two-phase constitutive model was developed for the material based on this relationship. The model attributes this overall composite behavior to the interaction of the brittle plastic matrix phase and the elastoplastic fiber phase.

The results of the model were input into a finite element program and compared to experimental test results from the FHWA flexure and shear tests of UHPC specimens. During

these tests, conventional reinforced concrete was replaced with unreinforced UHPC in standard AASHTO Type II girders and loaded to failure. The model was modified to take into consideration the effects of prestressing steel on strength, stiffness, and crack pattern, and produced very accurate results when compared with the available experimental data on both the global and local scale.

A maximum crack opening criterion for design purposes was introduced based on the UHPC design guidelines issued by the French Association of Civil Engineering (AFGC 2002) and were further expanded into a limiting strain criterion as follows:

Limiting crack criterion

$\omega_{lim} = 0.3$ mm $= 0.012$ in — for unreinforced UHPC sections

$\omega_{lim} = \min (L_f/4; h/100)$ — for reinforced UHPC sections

Limiting strain criterion

$\varepsilon_{lim} \leq \omega_{lim} / l_c = 1.5\ \omega_{lim} / h$ — for unreinforced sections

$\varepsilon_{lim} \leq \omega_{lim} / l_c = \min (3\ L_f / 8h; 3/200)$ — for reinforced UHPC sections

where:

- ω_{lim} = maximum admissible crack opening
- L_f = fiber length
- ε_{lim} = maximum admissible strain
- l_c = characteristic length = 2/3h
- h = height of structure

The limiting crack and strain criteria can be used to determine a lower bound on the limiting load for a member when coupled with the proposed model.

UHPC Section Design Formula, Strategy, and Criteria

The calculation of flexural strength of UHPC is similar to that of conventional reinforced concrete, but includes the contribution of the UHPC material in tension. In conventional reinforced concrete, the tensile contribution of the concrete is excluded from flexural strength calculations, because concrete exhibits a very low contribution before cracking and none beyond cracking. Also differing from conventional reinforced concrete design, UHPC employs a limiting crack criterion while conventional reinforced concrete design sets a limit on the compressive strain in the concrete.

The strategy adopted for the design of UHPC considers two limit states: service limit state (SLS) and ultimate strength limit state (ULS). The SLS design requirement limits the design member to no cracking, while the ULS follows the UHPC crack criterion guidelines developed by the AFGC. Using this strategy, an optimized section was developed by allowing variation in the section height and fixing the other variables to known or suitable quantities.

UHPC Simulation

The final phase of the model-based optimization process was the implementation into a real life simulation. The model was applied to a medium span, simply supported, prestressed

bridge girder and optimized using a combination of the material model, previously developed 3-D optimization techniques, and the crack limitation criterion. Optimizing a UHPC shape for a conventional bridge application yielded a smaller section than conventional bridge girders and integrated the riding surface into the girder (see Figure 3).

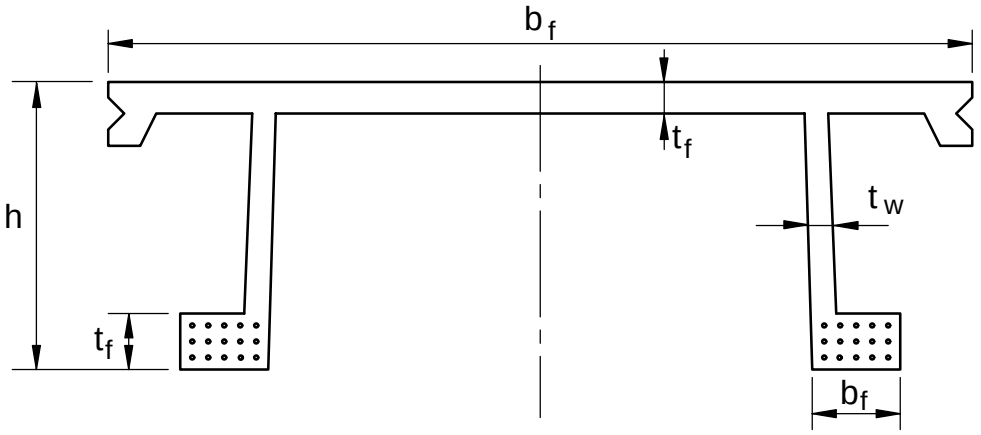

Figure 3. Optimized UHPC Bridge Girder

Limitations on the minimum thickness of the slab section were developed based on the service limit state 'no cracking' criterion; the section was capable of meeting the flexural strength requirements with thin slabs (2 in), but was unable to satisfy the SLS requirements with slabs thinner than 4 in. While the limitation to 4 in slab thickness is conservative, it serves as a safe lower bound in the absence of experimental data to support thinner slabs.

Preliminary Analysis

Slab systems differ considerably when compared to beam members due to the multi-dimensional nature of their configuration. The geometry of a slab makes it a highly redundant system, capable of undergoing significant rotations and deflections, maintaining a plastic moment and even redistributing bending moments prior to failure. As a result of this redundancy, slabs are very complex to analyze, not adhering to simple analysis procedures that can be used on other members such as beams and columns.

The determination of punching shear capacity of slabs historically has been based on experimental data obtained from laboratory testing, but no established models exist for the determination of actual behavior at failure in a slab (ASCE-ACI Task Committee 1974). This section presents the preliminary model developed for the determination of the punching shear capacity of UHPC slabs based on current ACI guidelines, modified to account for the properties of UHPC. Yield line analysis served as a basis for the determination of the failure mechanism and flexural strength. This preliminary analysis was used to establish the dimensions of the specimens, the supporting system, and the loading plate sizes.

The goal of this research effort was to determine guidelines for the design of UHPC to resist punching shear. However, in a slab system the mechanism of failure may be either flexure or punching. In order to quantify the limits of the punching failure load, a good understanding of the flexural failure load is also required. This will allow the design of specimens that fail primarily in punching shear. Preliminary analyses were performed on the two types of tested plates, namely the small plates (45 in x 45 in) and the large plates (7 ft x 12 ft).

Flexural Failure Mechanism

Yield Line Analysis

A common method for the determination of flexural capacity of concrete slabs is yield line analysis. In yield line analysis a collapse mechanism for the slab is determined, with consideration given to the boundary conditions, and used in conjunction with the principle of virtual work to determine the ultimate load of the slab system (Park and Gamble 2000). A generic representation of a probable collapse mechanism, involving formation of plastic hinges, for a simply supported slab with a uniformly distributed load is shown in Figure 4.

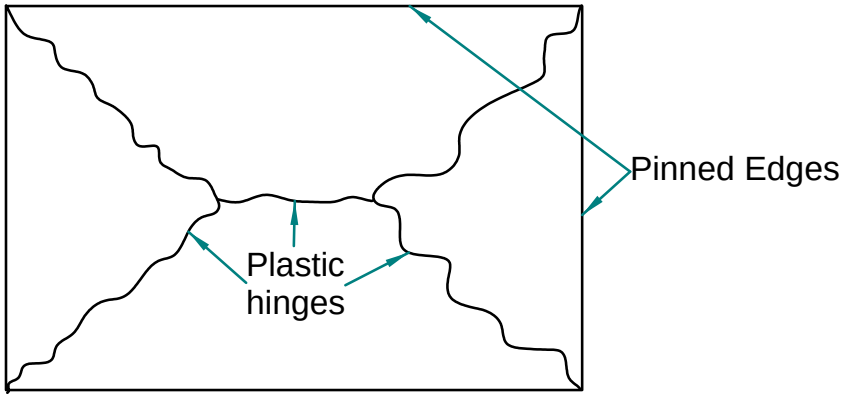

Figure 4. Generic Failure Mechanism for SS Slab with Uniformly Distributed Load

The use of yield line analysis requires knowledge of the plastic flexural capacity of the slab, and the results serve as an upper bound on the ultimate load of the system. The results of yield line analysis for a given slab are either correct or too high and are highly dependent on proper selection of a failure mechanism (Park and Gamble 2000).

The critical factors that must be considered when using yield line analysis are the distribution of the slab reinforcement, the ductility of the slab, and the conditions at the ultimate load. Yield line analysis is considered applicable for use in slab systems that are reinforced uniformly, typically in orthogonal directions; it is assumed that UHPC satisfies this requirement due to the randomly distributed steel fibers in the matrix. While conventional concrete uses rebar to provide the reinforcement, the steel fibers in UHPC serve as the micro-reinforcement in a similar manner. Slabs should also be sufficiently ductile to allow for plastic hinges to develop throughout the system; the degree of ductility or ductility factor is typically determined from the moment-curvature relationship as the ratio of the ultimate curvature (ϕ_u) to the yield curvature

(ϕ_y). The moment-curvature relationship for a reinforced concrete slab can be represented by a tri-linear shape consisting of an initially elastic portion, a linear section to yielding of the reinforcement, and a nearly horizontal region until failure as illustrated in Figure 5 (Park and Gamble 2000).

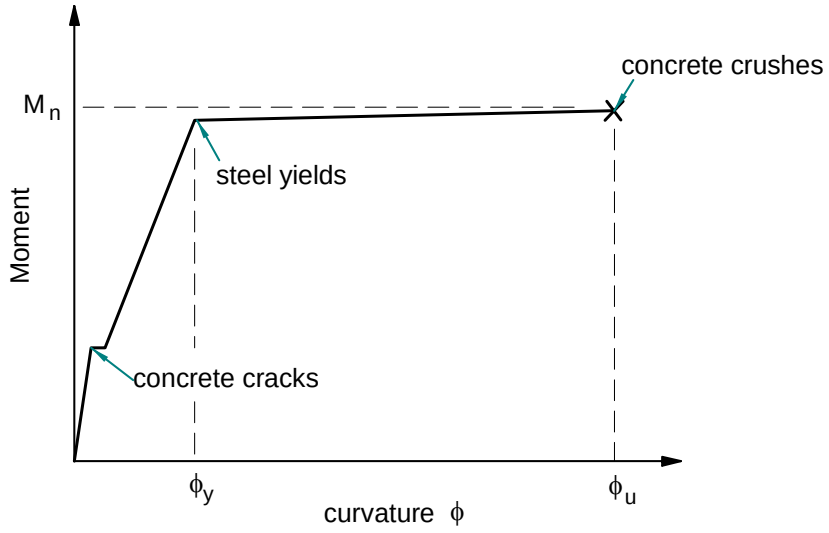

Figure 5. Typical Moment-Curvature Relationship for Reinforced Concrete Slab

Due to their highly redundant nature, slabs are capable of redistributing moments after the onset of cracking. When additional load is applied to the system, a large change in curvature occurs at the locations of first yielding and plastic hinges continue to form until there are a sufficient number of sections (rigid segments between yield lines) to result in failure of the slab; at this point the slab is no longer able to support additional load (Park and Gamble 2000). Yield line analysis allows the designer to place an upper limit of the capabilities of the slab, and design accordingly.

Flexural Strength

In order to properly perform a yield line analysis for UHPC slabs, an estimate of the flexural strength was required. A simplified model for the stress-strain relationship of UHPC based on the work of Park et al. (2003) is illustrated in Figure 6. Ductal® is assumed to be linear elastic in the compression zone, linear elastic in the tension region up to the cracking strain, and perfectly plastic to the limiting strain.

This stress-strain relationship was used to determine the flexural capacity, M_n, for various slab thicknesses using conventional sectional analysis methods; an iterative solution to balance the forces was required to determine the depth of the compression zone (Figure 7). The results of this analysis are summarized in Table 2.

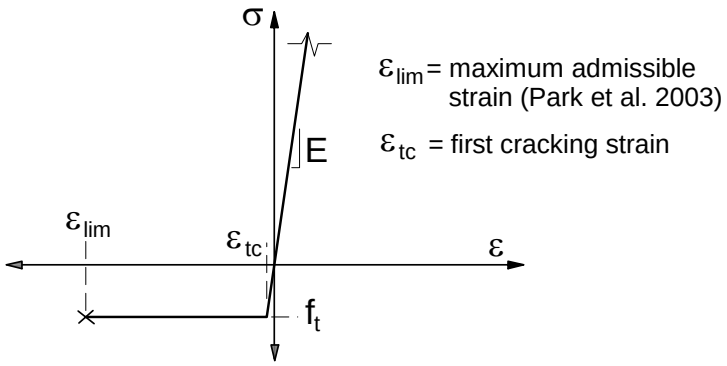

Figure 6. Stress vs. Strain Relationship for UHPC

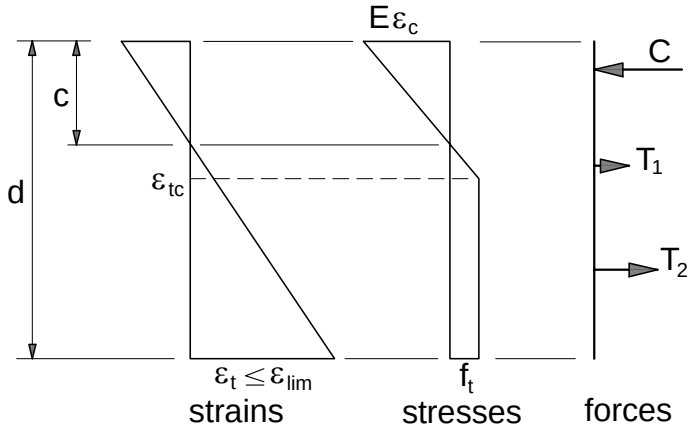

Figure 7. Section Model for UHPC Slab

Table 2. Flexural Strength (M_n) of UHPC Slabs

d in	ε_t strain	c in	T_1 kips	T_2 kips	C kips	M_n in-kip/ft
2	8.86E-03	0.301	0.18	22.06	22.24	**23.5**
2.5	7.09E-03	0.414	0.27	26.99	27.27	**36.2**
3	5.91E-03	0.535	0.39	31.77	32.15	**51.6**
3.5	5.06E-03	0.664	0.52	36.40	36.92	**69.4**
4	4.43E-03	0.800	0.67	40.90	41.57	**89.7**

Assumptions: (E = 7820 ksi, f_t = 1.1 ksi, ω = 0.012 in (0.3 mm), and b = 12 in)

To determine if UHPC was suitable for yield line analysis, the moment curvature relationships for various plate thicknesses were developed and are presented in Figure 8. For UHPC, specifically Ductal®, the flexural capacity in this analysis was limited by the limiting strain, ε_{lim}, on the tensile face as proposed in the report by Park et al. (2003).

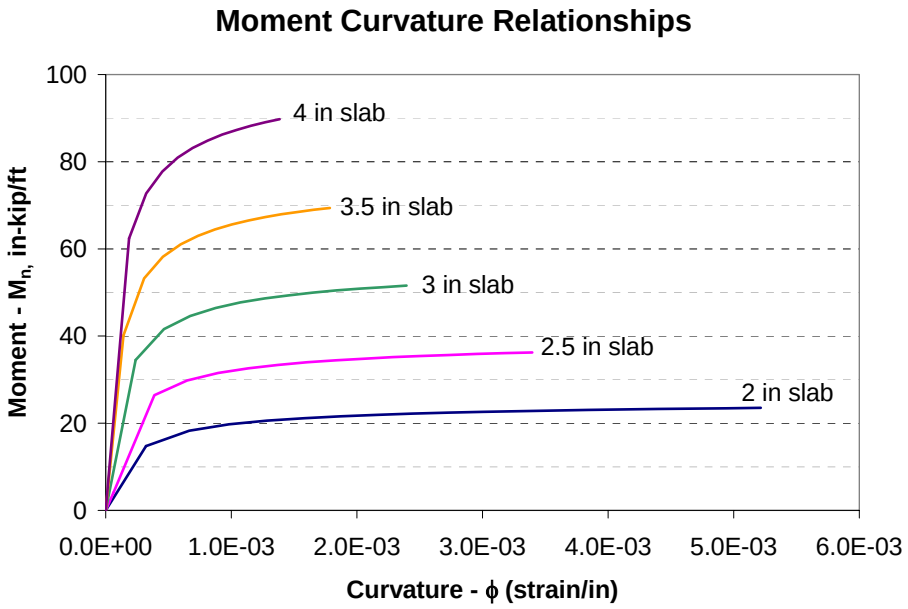

Figure 8. Moment-Curvature Relationship for UHPC

As illustrated in Figure 8, the moment-curvature relationship of UHPC can be approximately represented by a bi-linear relationship similar in shape to the tri-linear relationship of reinforced concrete. In UHPC there exists a distinct bend-over point which correlates to yielding of the reinforcing steel in conventional slabs, and the relationship also plateaus as it approaches the ultimate moment. For the 3.5 in and 4 in thick slabs, the region beyond the bend-over point does not adequately approach a horizontal plateau prior to the ultimate moment. These slab thicknesses were not included in this research effort, as this trend is not ideal for yield line analysis. However, the moment-curvature relationships for the 2 in, 2.5 in and 3 in slabs were deemed acceptable for use with yield line analysis.

Yield Line Analysis Results for UHPC

Based on the moment-curvature relationships developed, yield line analyses were performed for various slab thicknesses: 2 in, 2.5 in, and 3 in. The yield line analyses considered a distributed load over a small area (a x a) to simulate the effect of a small punch. Both pinned and fixed edge conditions were considered. Diagrams with the dimensions considered and three of the considered yield line patterns are shown in Figure 9. Detailed diagrams of each configuration are further illustrated in Harris (2005).

The results of the analyses demonstrated that a configuration of four fixed edges results in the highest load to cause a flexural failure, leaving a higher probability that a punching shear failure would occur for small punch sizes. The results are shown in Table 3 along with punching shear capacities, which are discussed in the following section.

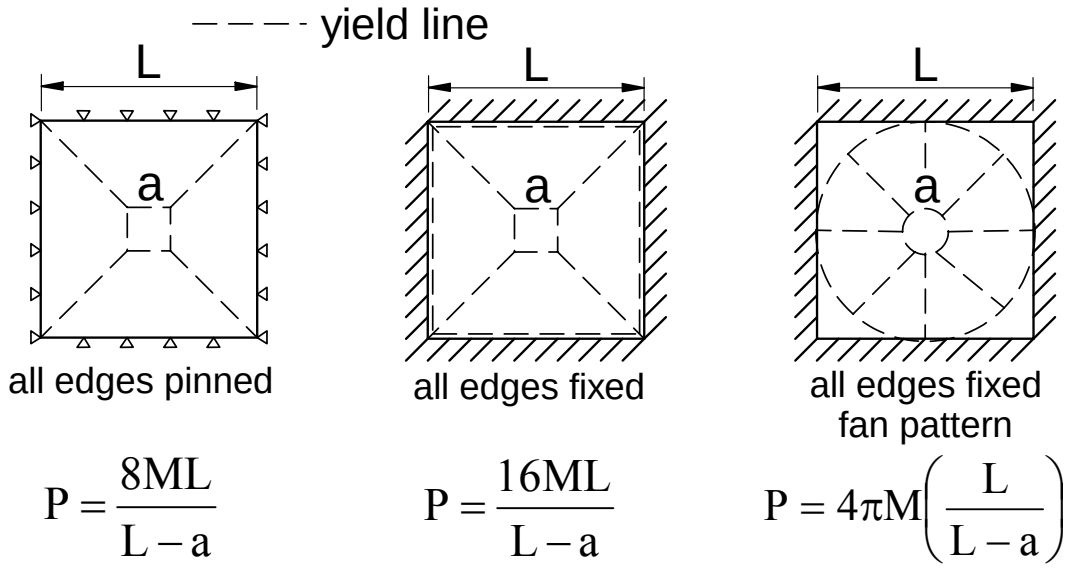

Figure 9. Primary Yield Line Analysis Configurations

Punching Shear Failure Mechanism

Tensile Strength of Ductal®

Conventional concrete is known to have a very low tensile capacity and to be incapable of sustaining load beyond initial cracking. For this reason, additional reinforcement is required to support tensile loads. UHPC, however, has been shown to exhibit significantly higher tensile strength than conventional concrete, both before and after cracking (Graybeal and Hartmann 2003). This tensile strength of UHPC is achieved as a result of the randomly oriented steel fibers acting as reinforcement on a micro level. After cracking has occurred, the steel fibers are capable of sustaining tensile loads until the fibers are pulled from the matrix and the section severs. The tensile strength in UHPC alone is not sufficient to carry the loads for many structural applications, but does allow for the designer to reduce the amount of reinforcement needed to resist tension. The testing conducted by Graybeal and Hartmann (2003) also indicates that there can be an improvement in the tensile strength of UHPC depending on the type and time of the curing regime.

ACI Approximation

The current ACI Building Code (ACI 2002) does not consider the tensile strength of concrete to contribute to flexure strength. However, for two-way or punching shear, the design equations in the ACI code include the term $\sqrt{f'_c}$ (psi) because it serves as a measure of the concrete tensile strength but is limited to a value of 100 psi (10,000 psi compressive strength concrete). This limit has been placed due to the limited amount of experimental test data on concrete with strengths above 10,000 psi compressive strength.

Since test data for high strength concrete are limited and UHPC does not contain reinforcement in the conventional sense, the ACI design equation presented below serves only as a rough foundation for the preliminary prediction of the punching shear capacity of UHPC slabs. The equation for punching shear that governs for a centrally loaded slab with a square punch as presented in ACI 318-02 is as follows:

$$V_c = 4\sqrt{f'_c}\, b_o d \tag{1}$$

where: f'_c = compressive strength of the concrete,
b_o = the perimeter of the critical section – critical perimeter,
d = the distance from extreme compression fiber to centroid of longitudinal tension reinforcement.

To roughly establish the punching shear capacity of UHPC slabs, the failure surface was assumed to be the same as that previously defined by ACI for punching shear. It was also assumed that the full tensile strength of the failure surface could be developed prior to punching. By replacing the tensile contribution of conventional concrete with the tensile capacity of Ductal®, the following equation was developed:

$$V_{Ductal} = (f_t + k_m) b_o h \tag{2}$$

where: V_{Ductal} = Punching shear capacity of Ductal slab
f_t = Brittle tensile strength of composite matrix - Park et al. (2003) ~0.1 ksi
k_m = Post-cracking tensile strength of composite matrix - Park et al. (2003) ~1.0 ksi
b_o = Critical perimeter (defined at a distance d/2 from loading area)
h = Slab thickness (differing from the ACI definition due to the lack of mild reinforcing steel)

This equation was used to determine the punching shear capacity of various slab thicknesses with varying punch sizes. Table 3 shows the ultimate loads for slabs with a 36 in by 36 in clear span with various punch sizes and slab thicknesses. The flexural capacities shown are for all edges fixed and all edges pinned. This preliminary analysis lead to the conclusion that to force failures in punching shear the punch would have to be quite small and the edges of the slabs would have to be fixed.

Due to the high cost of Ductal®, it was prudent to minimize the material used. It was determined that 3 ft by 3 ft slabs with fixed edges would provide a punching shear failure if the loading areas were sufficiently small. The expectation of the testing was that a series of slabs loaded over small areas would provide sufficient insight into the punching shear capacity of UHPC which could then be scaled up to accommodate practical applications.

RISA 3-D Model for Large Slabs

For the large slabs, in addition to determining punching shear strength and flexural strength based on yield line analysis, RISA-3D was used to model the behavior of the slabs while still in the elastic range. The primary purpose of these models was to determine the appropriate slab dimensions such that the length of the slab did not influence the stress distributions in the vicinity of the applied load. The goal of the large slab tests was to mimic the conditions in the top slab of the optimized double-tee, but it was desired to test the smallest possible slab size to minimize the specimen costs. An example of one of the models is shown in Figure 10; the contours shown represent the principal stresses on the bottom (tension side) of a slab loaded from the top and restrained on two edges. Based on the results of the modeling, it was determined that with an aspect ratio of two, the influence of the free edges would be minimized.

Table 3. Preliminary Analysis of Small Plates

Plate Thickness, in	Punch Size, in x in	Punching Shear Capacity, kips	Flexural Capacity With pinned edges, kips	Flexural Capacity With fixed edges, kips	
				X pattern	Fan pattern
2	1 x 1	26.4	15.3	32.3	25.4
	1.5 x 1.5	30.8	16.4	32.7	25.8
	2 x 2	35.2	16.6	33.2	26.3
	3 x 3	44.0	17.1	34.2	27.2
	4 x 4	52.8	17.6	35.3	28.1
2.5	1 x 1	38.5	23.6	49.7	39.2
	1.5 x 1.5	44.0	25.3	50.4	39.8
	2 x 2	49.5	25.6	51.1	40.5
	3 x 3	60.5	26.3	52.7	41.9
	4 x 4	71.5	27.1	54.4	54.4
3	1 x 1	52.8	33.6	70.8	55.7
	1.5 x 1.5	59.4	36.0	71.8	56.7
	2 x 2	66.0	36.4	72.9	57.6
	3 x 3	79.2	37.5	75.0	59.6
	4 x 4	92.4	38.6	77.3	61.7

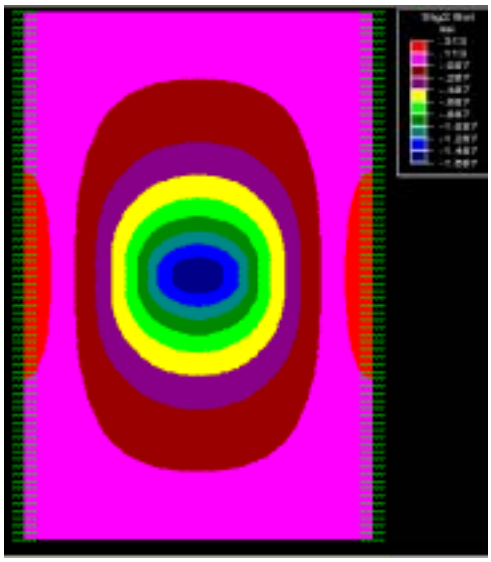

Figure 10. Risa 3-D Model of UHPC Slab (Restrained on Two Sides)

Review of Preliminary Analysis

The goal of this research project was to develop guidelines for the design of UHPC to resist punching shear. With slab systems there are two mechanisms of failure, flexure or punching shear, each with its own failure mode. In order to quantify the punching shear capacity of UHPC, specimens needed to be designed so that punching shear was the predicted mode of failure.

An upper bound approach, yield line analysis, was used to determine the flexural capacity of various slab configurations. The results demonstrated that the configuration with all sides restrained would require the largest load to cause failure, providing more opportunity to force a punching shear failure. The punching shear capacity of UHPC was estimated based on the ACI 318-02 design equations with modifications to account for the tensile capacity of UHPC. This preliminary analysis allowed for the determination of specimen sizes to be used in the experimental testing. These specimens were sized such that a punching shear failure could be achieved depending on the size of the loading area. This analysis served as the starting point for the experimental testing to be conducted. The actual test matrices are presented in the following sections.

In addition to the small tests, dimensions and support conditions for larger specimens, more representative of the top flange of the MIT optimized section, were also determined. The results of the larger plates are also presented in the following sections.

Laboratory Tests

In order to characterize the punching shear capacity of Ductal® a total of twelve 45 in by 45 in slabs and three 7 ft by 12 ft slabs were tested to failure. For the small slabs, the testing was performed on three slab thicknesses, 2 in, 2.5 in, and 3 in, with varying punch areas. Due to the uncertainty of the boundary between the flexural and punching shear failure mechanisms, the determination of the punch area used for any given test was based on the results of the previous tests. The large plates were loaded through a wheel patch, and were representative of the configuration of the top flange of the optimized double-tee section.

Specimen Fabrication

The twelve small slabs and three large slabs used in the testing were fabricated by Prestress Services, Inc. (PSI), in Lexington, Kentucky, in October and November of 2003. The slabs were poured from the excess Ductal® concrete material used in beam segments for the FHWA. The formwork was designed and constructed by PSI to produce 45 in x 45 in slabs with block-outs as illustrated in Figure 11, and 7 ft by 12 ft slabs with blockouts as illustrated in Figure 12. The block-outs were formed with pieces of PVC in the interior and lifting eyes in the corner locations; the lifting eyes were installed to allow easy lifting and positioning of the slabs. The block-outs were necessary to bolt the edges of the slabs down to the test frames to create fixed edge conditions.

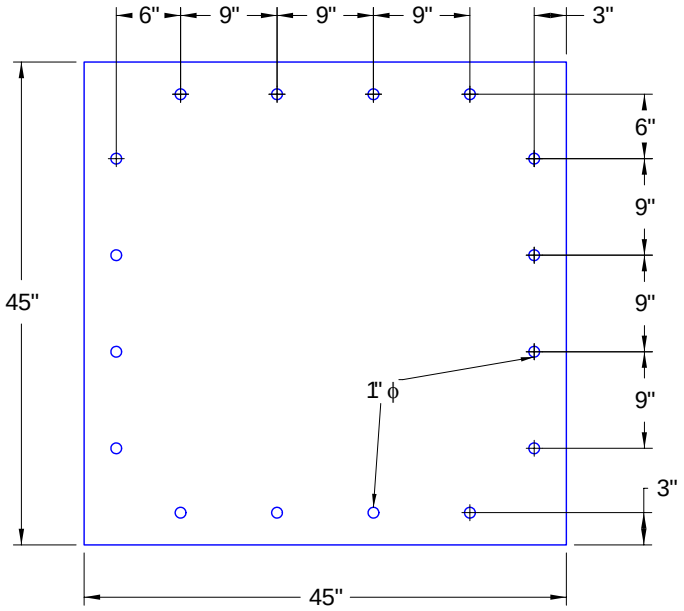

Figure 11. 45 in x 45 in Slab Layout with Blockouts

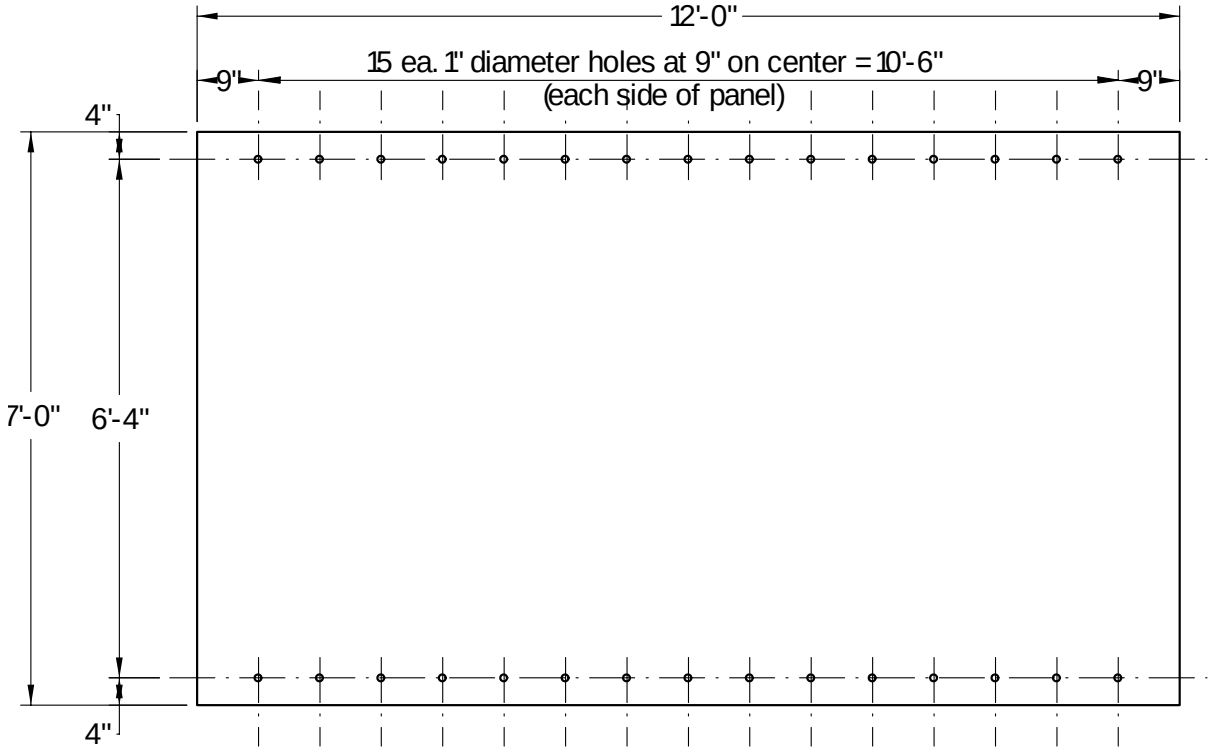

Figure 12. 7 ft by 12 ft Slab Layout with Blockouts

The slabs were poured using a trough system that was similar in width to the slab width. A mix truck was used to pour the Ductal® into the trough, which was pushed across the forms in a linear manner to fill the formwork. The slabs were covered with plastic and then subjected to an initial cure followed at a later date with a post-cure heat treatment. This curing regime was demonstrated by Graybeal and Hartmann (2003) to provide improved tensile strength.

After curing and heat treatment, the slabs were stored in preparation for transportation to the Virginia Tech Structures and Materials Laboratory. All of the slabs exhibited a very smooth surface on all sides that were in contact with the formwork, but the surfaces in contact with the plastic tarp were rough to the touch. A number of the slabs were poured in excess of the required thickness due to the lack of precision in the trough system used. However, these slabs were deemed acceptable for testing. In addition, the bolt holes on two of the slabs were not placed properly due to error in formwork fabrication and required modifications to the frame to compensate.

Cylinders were made by the quality control personnel of PSI. These cylinders were transported to the FHWA's Turner-Fairbank Laboratory for testing. The results of the material tests were provided by FHWA and are shown in Table 4 for the pours in which slabs were cast.

Table 4. Summary of Material Properties

Compressive Strength – No Modulus Test (ksi)	32.1
Compressive Strength – Modulus Test (ksi)*	31.6
Tensile Strength (ksi)	1.6
Elastic Modulus (ksi)	7857

*Compressive strength – modulus test was loaded in the elastic region to record the modulus and then loaded to failure. Compressive strength – no modulus test was directly loaded to failure.

Experimental Setup

Historically concrete slabs have been tested as simply supported systems loaded from above. A very limited number of experiments have been conducted on fully restrained slab systems, making the frame design challenging. However, a series of tests conducted by Keenan (1969) served as a good example of how to effectively fully restrain a slab. The effective restraint of the slab edges was crucial to the experiment because a simply supported slab requires a much smaller load to cause a flexural failure; this decrease in load would lower the probability of achieving a punching shear failure. The restraint system employed in the study by Keenan (1969) used a system of channels and angles to prevent deflection or rotation of the edges and served as the foundation for the restraint system used in this experiment.

Frames

For the small slabs a steel frame was utilized due to ease of construction, fabrication and reconfiguration possibilities. A sketch of the final frame configuration is shown in Figures 13 and 14, with the actual frame shown in Figure 15. The slabs were supported by W14 x 82 beams bolted to W14 x 82 columns that were bolted to the reaction floor. The rotations and deflections

of the slabs were restrained by L4x3x1/2 angles on the perimeter and C4x7.25 channel sections on top of the slab bolted through the slab and the supporting beam flanges. A detail of the restraint system is illustrated in Figure 16.

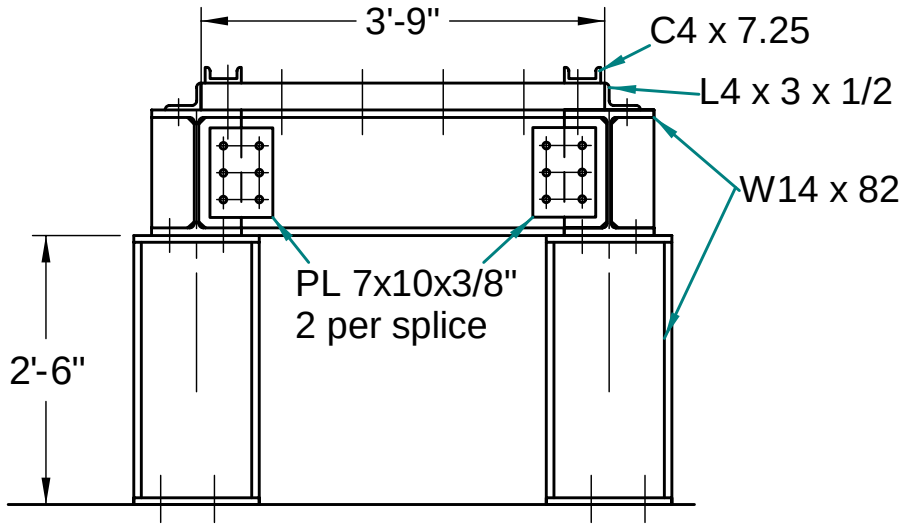

Figure 13. Elevation 1 of Frame

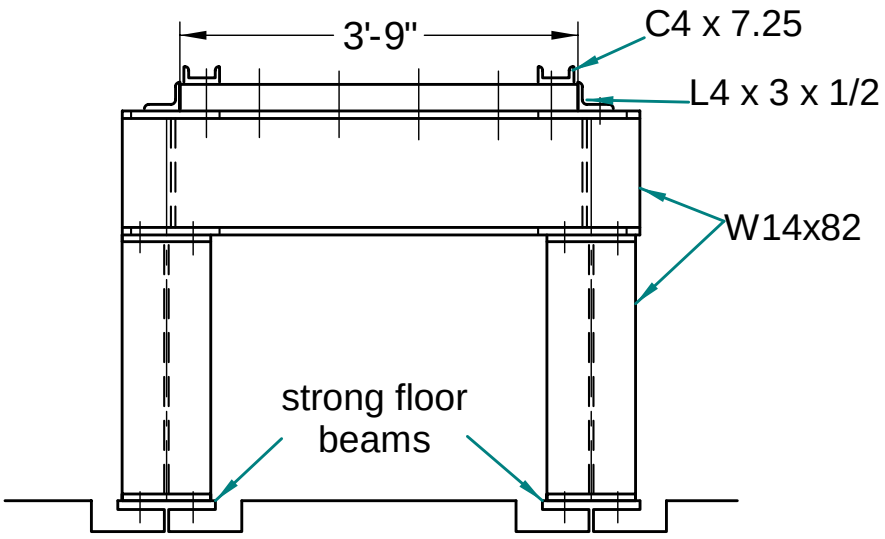

Figure 14. Elevation 2 of Frame

Figure 15. Frame for Small Slab Tests

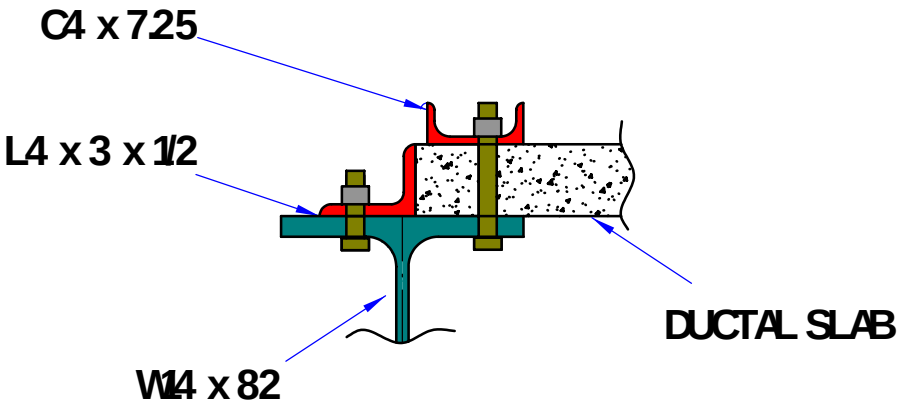

Figure 16. Detail of Frame Restraint System

The frame used for the large slabs used the columns and beams from the small frame, along with additional columns and beams. The load was applied from above with a standard loading frame. This frame is shown in Figure 17. For the large slab, the restraint conditions were varied from partially fixed to pinned. The edges of the partially fixed slabs were restrained between a channel and the supporting beams. Bolts, passing through blockouts in the slab every 9 in were tightened with an impact wrench. For the pinned conditions, the slab rested on the supporting beams, and bolts were passed through the blockouts to attach the slab to the beams. However, these bolts were not tightened, so the slab edges were free to rotate.

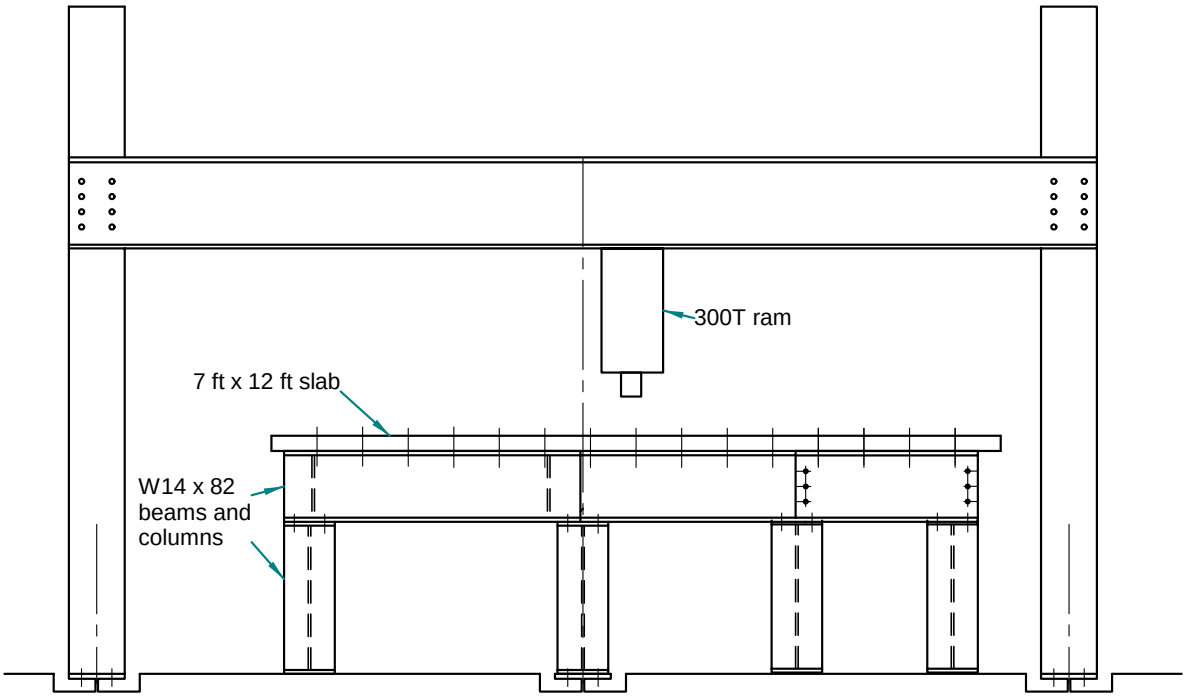

Figure 17. Frame for Large Slab Tests

Small Slab Instrumentation

The small slabs were loaded from the bottom using a 300 ton ram and a 150 kip load cell. The slabs were loaded with the formed surface facing up; this allowed for observation of tensile crack propagation on the smooth face of the slab.

Each of the slabs was outfitted with several strain gauges on the top and bottom face to monitor the strain response. The placement of the strain gauges was based on the likely location of crack formation, and was adjusted for each new test slab based on the cracking seen in the previously tested slab. The strain gauge nomenclature was based on a relative reference with respect to the laboratory. The expected flexural failure mechanisms for a slab with all edges fixed against rotation and with a point load at the center are illustrated in Figure 9. The strain gauges were positioned in directions that were perpendicular to the predicted crack pattern; the goal was to observe the strain response and compare the results to the limiting strain values proposed by Park et al. (2003). The general placement locations for strain gauges for the top and bottom faces are illustrated in Figure 18. It should be noted that the final strain gauge placement was dependent on the predicted failure mechanism determined prior to testing as well as the failure mechanism predicted based on previous tests.

A maximum of nine strain gauges were used on each slab. Vishay Micro-Measurements strain gauges were used on all slabs with CEA-06-500UW-350 (1/2 in – 350 Ω - G.F. = 2.100) gauges used on the first 11 slabs and CEA-06-500UW-120 (1/2 in – 120 Ω - G.F. = 2.085) gauges used on the final slab. Prior to mounting the gauges on the slab, the surface was ground

with a masonry grinding pad to ensure a smooth surface for adhesion. The gauges were mounted directly to the Ductal® surface using Vishay Measurements Group M-Bond 200 adhesive.

To apply and measure the loads during testing, a ram/load cell combination as illustrated in Figure 19 was used. Steel plates of various sizes were used as the punch area and were placed on top of the loading area to transfer the load from the ram to the plate specimen. A list of the punch sizes used is provided later. To measure the displacement of the slab at the point of load application, one wire pot displacement transducer was attached to each side of the ram to provide a redundant system for measuring displacements. The wire pots were not attached directly to the slabs due to the difficulty in boring into the slab with a conventional drill and masonry bit.

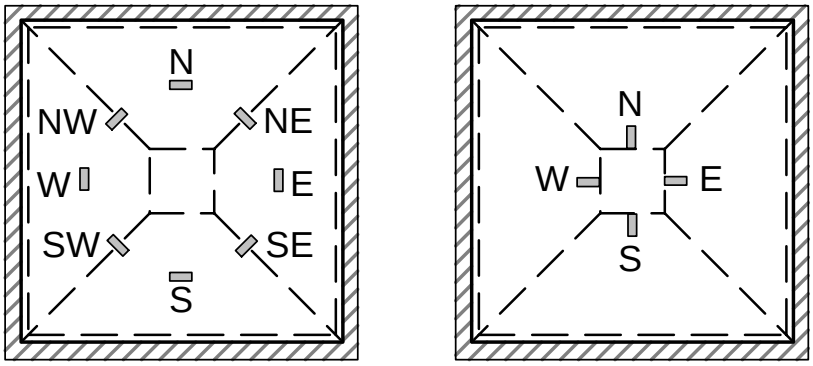

(a) Top Face **(b) Bottom Face**

Figure 18. Strain Gauge Placement Configurations

During the initial series of tests, two linear variable differential transducers (LVDTs) were mounted on the frame and positioned to record the displacement at the top of the angles on perpendicular faces. The LVDTs were used to verify the stiffness of the angles, but were not used after the initial series of tests due to the negligible deflections observed. Due to the number of unknowns in the design of the frame, assumptions were made about the acceptable deflections of the angles.

The output was recorded using a Vishay Measurements Group System 5000 Scanner. The software used for recording and processing the test data was Smart Strain. For all of the tests, the data were recorded on a continuous basis with sampling rates varying from 1-2 recordings per second; the software allowed for real-time monitoring of results during testing.

Large Slab Instrumentation

The large slabs were instrumented with the same type of strain gauges used on the small slabs. The pattern of gauge application was varied due to the unexpected mode of failure on the first tested plate. Figure 20 illustrates the strain gage positions in the first, second and third plate tests. At each indicated location, one gauge was affixed to the top surface and one to the bottom surface. It was hoped that a strain profile could be measured and equated to the moment in the slabs at each location.

Deflections were measured at midspan directly under the load with LVDTs. LVDTs were used to measure the rotation of the edges of the slabs for the restrained edge tests to investigate if edge rotations were occurring. Finally, the load applied by the ram was measured with a 150 kip load cell placed between the ram and the loading frame.

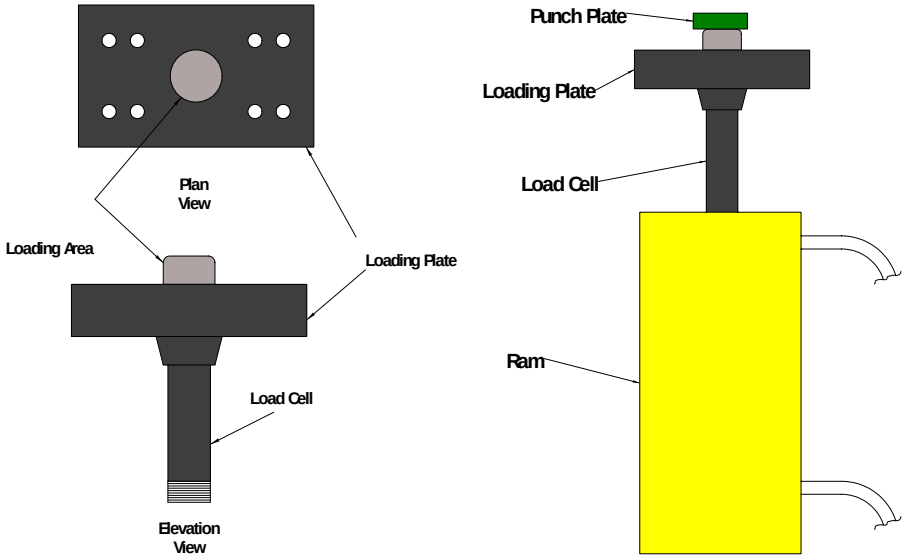

Figure 19. Ram/Load Cell Combination

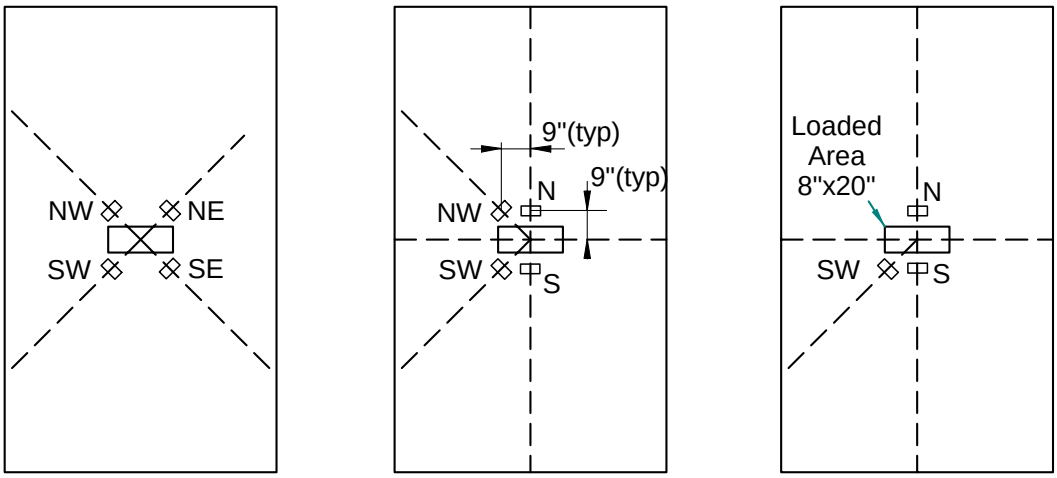

Figure 20. Gauge Locations on Large Slab Tests

Test Matrices

Test Parameters and Series Details

The testing was conducted on three series of small slabs (2.0 in, 2.5 in, and 3.0 in thick) with varying punch sizes and one series of large slabs loaded through a wheel patch. One of the goals of the small slab testing was to determine the boundary between a punching shear failure and a flexural failure with the majority of tests failing in punching so strength could be characterized. The philosophy in determining the punching area was to produce a punching shear failure in the first test of each series based on the preliminary analysis results. The subsequent tests varied the plate area to produce failures on both sides of the spectrum, punching shear and flexure, which would help define the boundary between the two failure mechanisms.

Series 1: 2 in Slabs

The first series tested were the 2.0 in thick slab specimens. These slabs were tested first due to the limited knowledge of the behavior of Ductal® in punching shear and the low probability that a 2.0 in slab would be used in a bridge application based on the study by Park et al. (2003). Initially it was intended to test four slabs in each series, but one of the 2.0 in slabs was evaluated as a 3.0 in slab in Series 3 because it was poured in excess of the desired thickness. The test matrix for Series 1 is shown in Table 5.

Table 5. Series 1 Matrix -2.0 in Slabs

Test No.	Punch Area in^2	Punch Dimensions in x in	Predicted Failure Load kips	Predicted Failure Mechanism
1	2.25	1.5 x 1.5	25.8	Flexural
2	4.0	2.0 x 2.0	26.3	Flexural
3	1.0	1.0 x 1.0	25.4	Flexural

Series 2: 2.5 in Slabs

The specimens evaluated in Series 2 were 2.5 in thick slab specimens. Initially only three slabs were tested because the bolt holes were misaligned on the fourth due to improper placement of the block-outs during casting, but a total of four slabs were tested after modifications were made to the frame. The test matrix for Series 2 is shown in Table 6.

Table 6. Series 2 Matrix - 2.5 in slabs

Test No.	Punch Area in^2	Punch Dimensions in x in	Predicted Failure Load kips	Predicted Failure Mechanism
1	4.0	2.0 x 2.0	40.5	Flexural
2	9.0	3.0 x 3.0	41.9	Flexural
3	2.25	1.5 x 1.5	39.8	Flexural
4	6.25	2.5 x 2.5	51.9	Flexural

Series 3: 3 in Slabs

The last specimens evaluated in Series 3 were 3.0 in thick slab specimens. These slabs were the most critical in the testing series because 3.0 in was the minimum allowable top flange thickness for the optimized double-tee according to the study by Park et al. (2003). In Series 3 a total of five slabs were tested due to the additional slab gained from the excessive thickness of a 2.0 in slab. The test matrix for Series 3 is shown in Table 7.

Table 7. Series 3 Matrix - 3.0 in slabs

Test No.	Punch Area in^2	Punch Dimensions in x in	Predicted Failure Load kips	Predicted Failure Mechanism
1	6.25	2.5 x 2.5	58.6	Flexural
2	2.25	1.5 x 1.5.	56.7	Flexural
3	1.0	1.0 x 1.0.	52.8	Punching
4	4.0	2.0 x 2.0.	57.6	Flexural
5	3.06	1.75 x 1.75	57.1	Flexural

Series 4: Large Slabs

The specimens evaluated in Series 4 were the large 7 ft by 12 ft slabs. As previously mentioned, these slabs were designed to represent the top flange of the optimized double-tee girder. They were supported on the two long edges, while the two short edges were unsupported. The original plan was to test all three slabs with the long edges fixed against rotation, and test three slab thicknesses, 2 in, 2.5 in, and 3 in. Unfortunately, all three slabs were cast approximately 3 in thick. So, two slabs were tested with the edges fixed and one slab was tested with the edges pinned. Table 8 shows the test matrix.

Table 8. Test Matrix for Series 4 – Large Slabs

Test No.	Plate Size ft x ft	Load Patch Size, in x in	Average Plate Thickness, in	Boundary Conditions	Predicted Failure Load, kips	Predicted Failure Mode
1	7 x 12	8 x 20	3.05	Fixed	71.0	Flexure
2	7 x 12	8 x 20	2.80	Fixed	60.2	Flexure
3	7 x 12	8 x 20	2.70	Pinned	28.0	Flexure

Test Procedures

Testing Small Slabs

After the slabs were positioned in the frame and bolted in place, the slabs were tested with a 300 kip ram with pressure applied through a hydraulic hand pump. The slabs were loaded in 3 to 5 kip increments and after each increment cracks were marked on the specimen. The marking for cracks continued until the load was within 6 kips of the predicted failure load, which was based on the preliminary analysis and previous test results. For the punching shear failures, the slabs were loaded until a decrease in load was observed in the load-deflection curve following the peak load. The criterion for termination of loading on the flexural failures was more subjective and was determined from the load-deflection curve as the point at which the curve reached a plateau after the peak load.

Testing Large Slabs

After the slabs were placed on the supporting beams the edges were bolted to the beams. As discussed earlier, the first two slabs were restrained between a channel above and the supporting beam below, and the bolts were tightened. The third slab was bolted to the support beams, but the bolts were left loose to allow edge rotation. The load was applied at the center of the slab through two sections of a rubber tire, filled with a semi-rigid polymer as shown in Figure 21. Steel plates were placed on top of the polymer, and a short I-beam was used to distribute the load from the ram to the two plates. The loading area was approximately 20 in by 8 in

The slabs were loaded by a 300 kip ram. The load was applied in increments of approximately 0.5 kips. Cracking was strongly indicated by loud noises, at which time the slab would be visually examined for cracks. Alcohol in spray bottles was used to apply a mist to the bottom surface of the slab to assist in the detection of cracks. Cracks were marked and widths were measured with a crack comparator card. Loading continued until the slab was deforming significantly, with significant decreases in load.

Figure 21. Tire Patch Used to Load Large Slabs.

RESULTS

Overview

The slabs tested in this research effort failed in one of two mechanisms: punching shear or flexure. This section summarizes the results from each test and discusses the failure mechanisms. The results of each test are then compared to the predicted response from the preliminary analysis and other proposed equations for predicting punching shear capacity.

Failure Mechanisms

A punching shear failure is typically a brittle failure that occurs with limited warning, and for the Ductal® slabs this occurred when the applied load dropped suddenly at the same time a cone of concrete punched though the slab. An example of a typical punching shear failure for Ductal® is shown in Figure 22. Cracking on the tensile face began near the center and radiated out to one of the edges, and as the load was increased, the cracking migrated to the opposite face. For most of the slabs, the direction of cracking tended to be in one direction; this led to the hypothesis that the fibers were not as randomly oriented as expected. This phenomenon was attributed to the casting technique used in which the slabs were poured in a uniaxial direction with a trough system, resulting in alignment of the fibers parallel to the direction of pour. This enabled the cracks to form between the fibers (Figure 23). This theory is in agreement with the trend described by the AFGC recommendations (2002) in that the fibers tend to align with the direction of the pour and along the formwork. Failure of the slab occurred when the cone of failure radiating outward from the point of load application pushed up through the slab body. At failure the slab was no longer capable of taking additional load and the majority of the cracking had occurred in one direction, as illustrated in Figure 24.

(a) Tensile Face of Typical Slab Failing in Punching Shear

(b) Loading Face of Typical Slab Failing in Punching Shear

Figure 22. Typical Punching Shear Failure for Ductal®

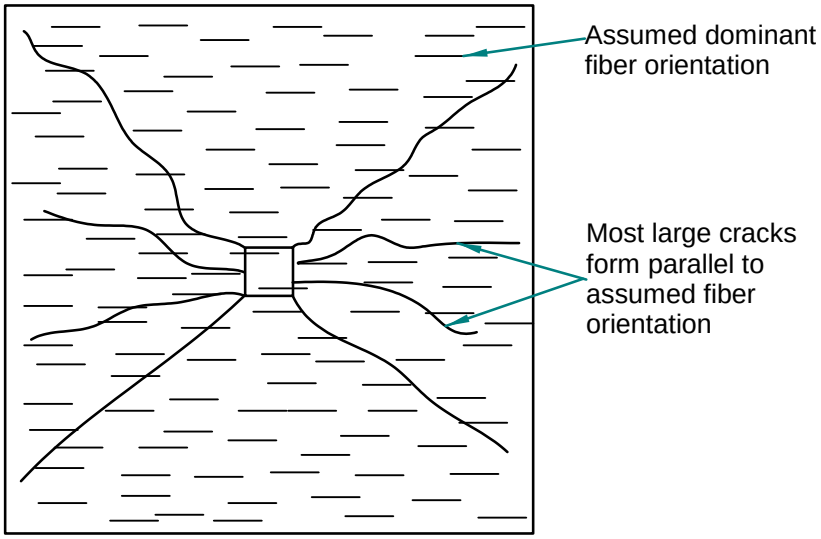

Figure 23. Fiber Orientation vs. Crack Pattern

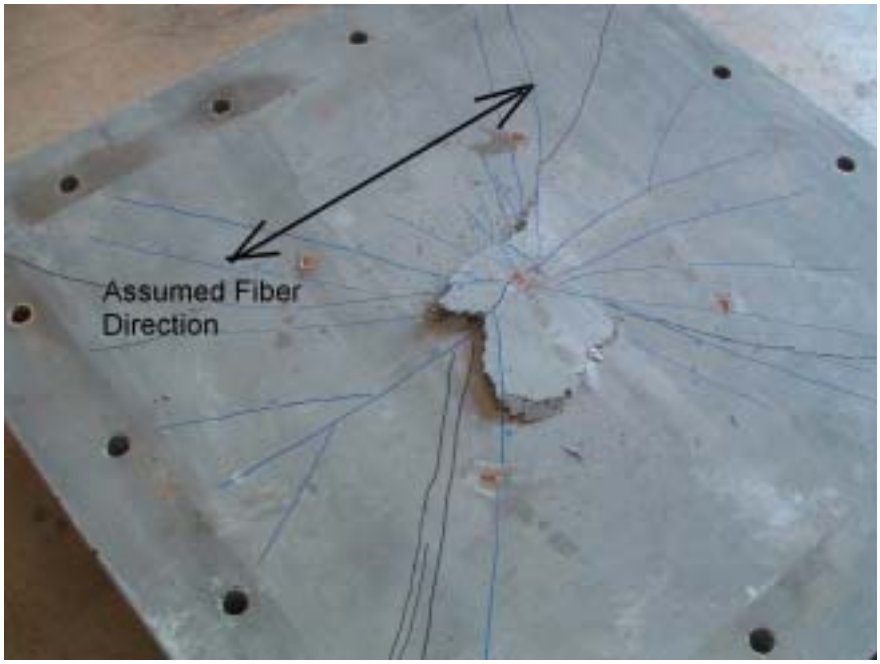

Figure 24. Typical Crack Pattern for Punching Shear Failure

Contrary to punching shear failures, a flexural failure is a gradual failure that allows for the support of a reduced load after the formation of plastic hinges in the slab. A slab is capable of additional deformation, while maintaining a peak load, which is considered a more ductile failure, the preferred failure mechanism in design. An example of a typical flexural failure for Ductal® is shown in Figures 25 and 26 showing the tensile face and the loading face, respectively.

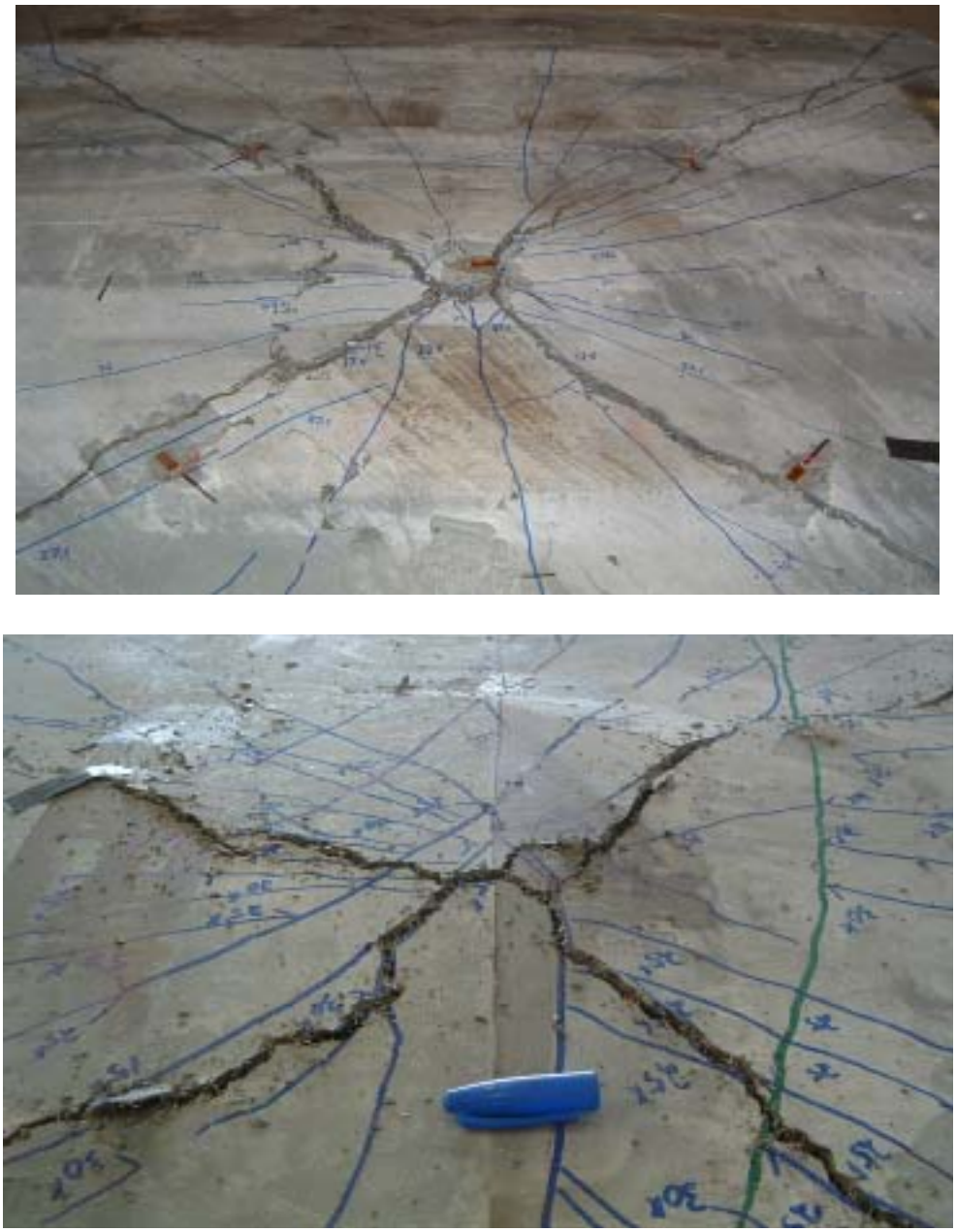

Figure 25. Crack Patterns on Tension Faces of Specimens with Flexural Failures

Figure 26. Cracking Pattern on Loaded Face of Specimens with Flexural Failures

Similar to the punching shear failure mechanism, cracks initially formed near the center of the slab on the tensile face and radiated to the edges. As loading continued, the cracks along the diagonals on the tensile face widened and extended through the slab thickness to the loading face with additional cracks forming at the fixed support on the loading face. The slabs that failed in flexure reached a peak load, which was maintained briefly, followed by a gradual decrease in load while continuing to deform.

All of the slabs tested failed at loads lower than predicted in both flexure and punching shear. The overestimation of the flexural failure loads can be attributed to a number of factors including the use of yield line analysis, inaccurate assumption of moment capacity, and the degree of fixity at the supports. Yield line analysis serves as an upper bound on the load carrying capacity of the slabs considered. The use of yield line analysis requires knowledge of the moment capacity in orthogonal directions, but based on the crack patterns observed during testing, the two were not the same as assumed in the yield line analysis. Full restraint of the slab edges was essential for forcing punching shear failures according to the preliminary analysis because it requires the largest load to cause a flexural failure. Investigation of the slabs after testing showed that the flexural hinges at the support face were not as distinct as the diagonal hinges, indicating that the slabs may not have been fully restrained along the edges. This could have also resulted in a lower load than predicted from the yield line analysis of a fully restrained slab.

The failure mode of all three large slabs was flexure. Initial cracking developed along the midspan of the slab near the loading point. The cracks then propagated toward the free ends of the slab. Additional cracks developed close to the load point near the middle of the slab, and

then propagated toward the edges of the free ends. Figure 27 illustrates a typical cracking pattern. Yield line analysis indicated that flexural cracking for the slabs that were fixed on the edges should form in more of a fan pattern than what was observed. The lack of fan pattern type cracking could indicate either less than full restraint of the edges or, as discussed for the small slabs, a dominant direction of fiber orientation which would result in the flexural strength in one direction of the slab being smaller than in the orthogonal direction. At the end of each test, several of the cracks opened quite widely and the deflections increased significantly. Then, one dominant crack opened and the concrete on the compression face above the crack crushed and spalled. At this time loading was discontinued.

Figure 27. Typical Cracking Pattern on Bottom Surface of Large Plate Specimens.

Testing Results

Series 1 Results

The slabs tested in Series 1 were all approximately 2.0 in thick specimens, and results are shown in Table 9. Note that the predicted failure loads are slightly different than those shown in Table 3, because they reflect the actual measured thicknesses of the tested slabs. Series 1 consisted of three tests because one of the slab specimens was poured in excess of 2.0 in and was deemed unacceptable for testing as a 2.0 in slab, but was tested in Series 3 as a 3.0 in slab.

Table 9. Series 1 Test Results

			Predicted			Actual		
Test No.	**Slab Thickness in**	**Punch Plate Size in**	**Punching Failure Load kips**	**Flexural Failure Load kips**	**Failure Mechanism**	**Failure Mechanism**	**Failure Load, kips**	**Average Maximum Deflection$_{(midspan)}$ in**
1	2.17	1.5	35.0	30.3	Flexure	Punching	23.3	.724
2	2.32	2	44.1	35.0	Flexure	Punching	27.2	.796
3	2.12	1	29.1	28.5	Flexure	Punching	22.6	No data

The results from Series 1 indicate that a very small loading area is required to force a punching shear failure in Ductal® slabs. As shown in Table 9, all of the Series 1 specimens tested failed in punching shear. The failure mechanism was abrupt, ending with the slab not capable of supporting additional load, and a cone of concrete broken through the slab. The response is best illustrated with a load-deflection curve as shown in Figure 28. As expected, the slabs were capable of undergoing a significant amount of deformation prior to failure, around 3/4 in which equates to approximately L/48. It appears from the load deflection plot that the slabs were approaching a flexural failure, but the punching shear failure occurred first.

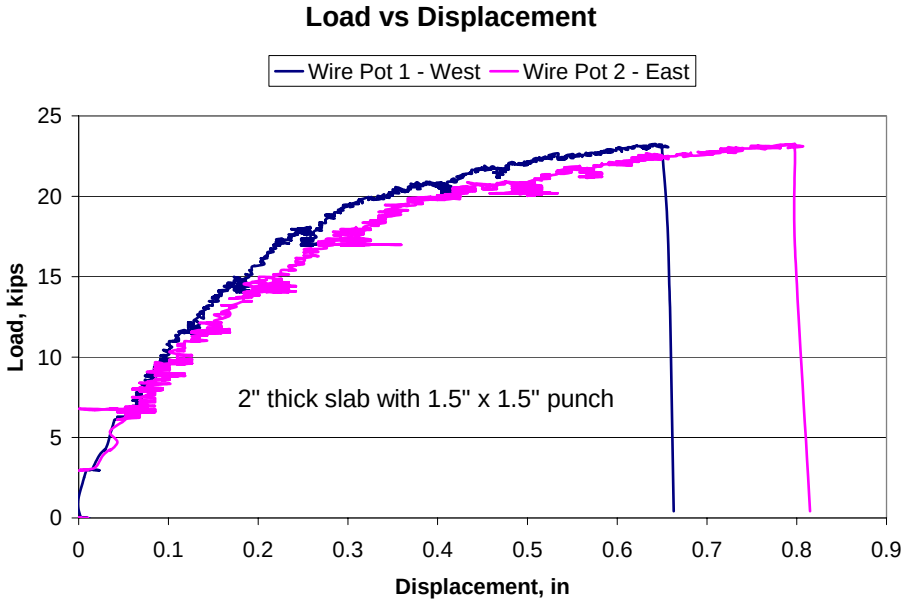

Figure 28. Typical Load vs. Displacement Curve for Series 1 - Slab #1

The strains recorded from the strain gauges were highly dependent on the crack pattern observed during the test. The strain values recorded by the gauges located on the diagonals of the slab varied depending on the path of the diagonal cracking, with high tensile strains observed when the cracking passed near or through the gauge location. An example of this trend is illustrated in Figure 29 with the NW strain gauge experiencing significantly higher tensile strain than the other gauges; a major crack likely formed underneath or within very close proximity to this gauge. It can also be observed that the other strain gauges experienced increases in tensile strain, but at a much higher load than the NE strain gauge. This likely resulted from the strain induced at the gauge from the growth of a crack that previously did not have a major influence on the gauge. Based on previously stated limiting strain criteria, the limiting strain for a 2 in thick slab is 8860με. This correlates well with the maximum measured strain.

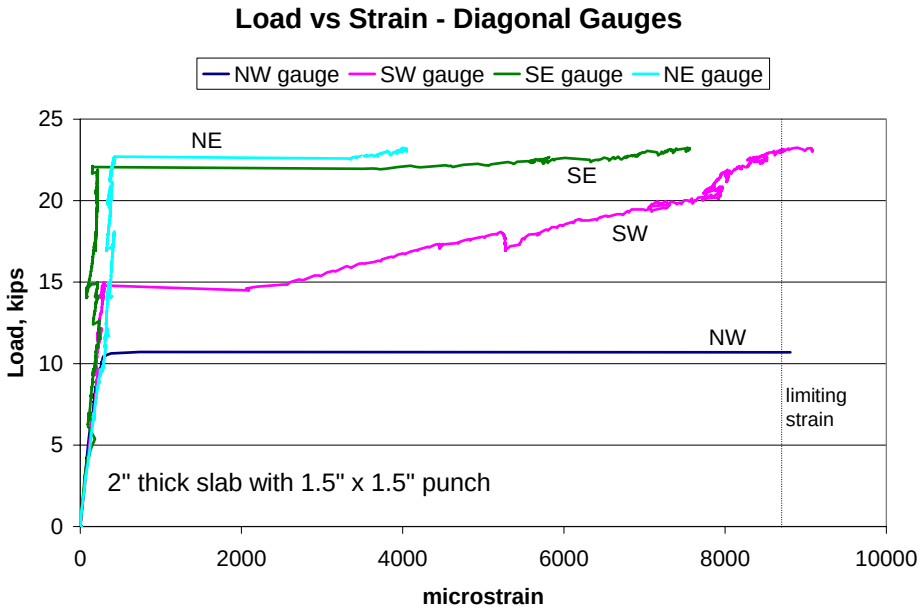

Figure 29. Typical Load vs. Strain in Gauges on Diagonals for Series 1 – Slab #1 (Tensile Face)

For gauges placed in the orthogonal directions to the spans, the general trend was similar to that observed along the diagonals, with strain response dependent on crack location. This is illustrated in Figure 30. The strain response of the gauges on the loading face was different as a result of the gauges being in compression until just prior to failure; compression is shown as a negative strain value. The general trend observed in Series 1 is illustrated in Figure 31. The compressive strain increases proportional to load increases until failure, after which the compressive strain is relieved as the loading area punches through the slab.

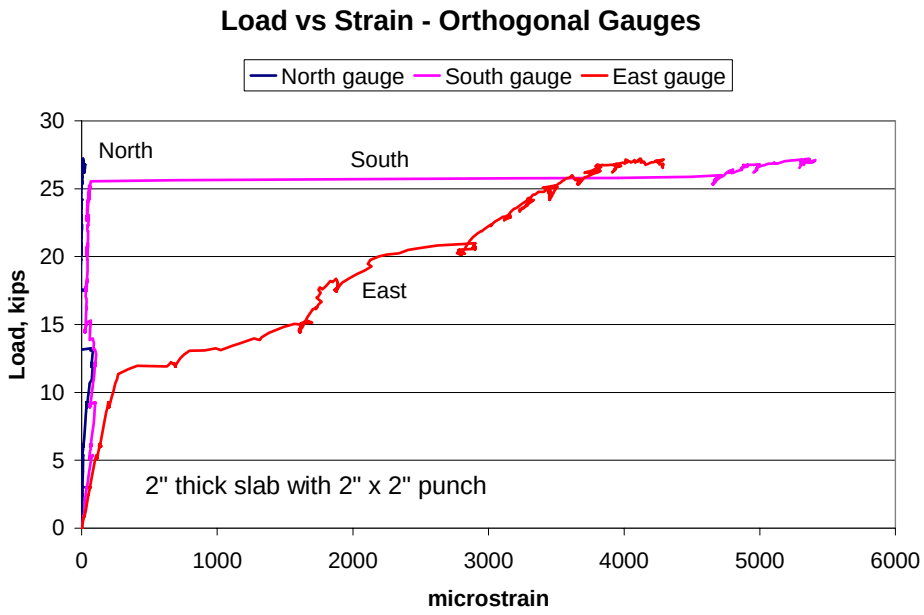

Figure 30. Load vs. Strain in Orthogonal Gauges for Series 1 – Slab #2 (Tensile Face)

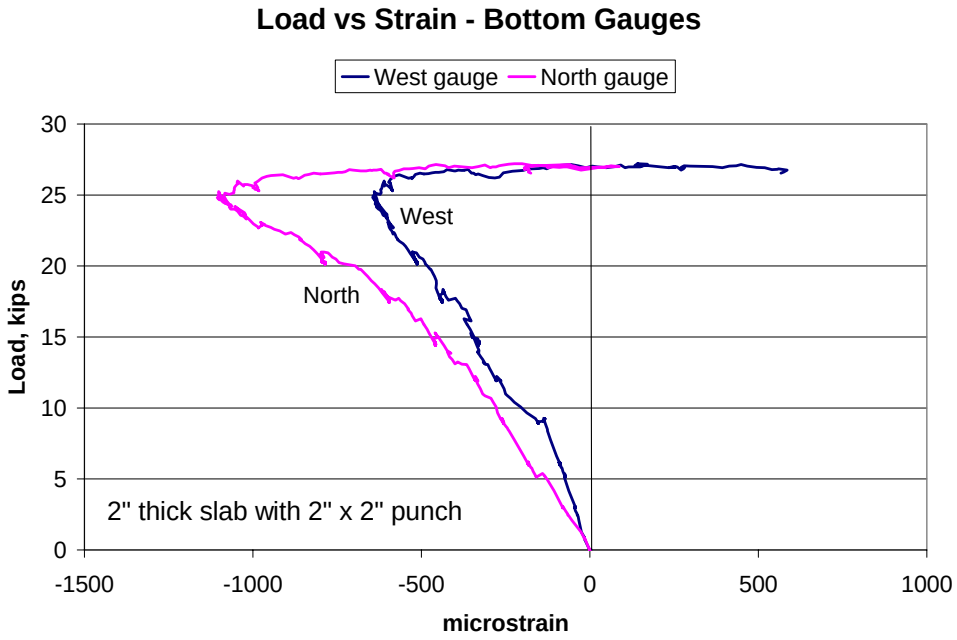

Figure 31. Typical Load vs. Strain for Series 1 – Slab #2 (Loading Face)

Series 2 Results

The four slabs tested in Series 2 were all approximately 2.5 in thick specimens. The results are shown in Table 10.

Table 10. Series 2 Test Results

			Predicted			Actual		
Test No.	**Slab Thickness in**	**Punch Plate Size in**	**Punching Failure Load kips**	**Flexural Failure Load kips**	**Failure Mechanism**	**Failure Mechanism**	**Failure Load kips**	**Average Maximum Deflection$_{(midspan)}$ in**
1	2.61	2	53.1	44.0	Flexure	Punching	33.0	0.57
2	2.58	3	63.2	44.5	Flexure	Flexure	35.9	2.11
3	2.54	1.5	45.2	41.1	Flexure	Punching	30.5	1.26
4	2.76	2.5	64.0	49.9	Flexure	Flexure	34.2	1.87

As a whole, the results observed from Series 2 were comparable to those from Series 1. While all of the specimens tested in Series 1 failed in punching shear, the specimens tested in Series 2 experienced both flexural and punching shear failures. The punching shear and flexural failures were similar in nature to the descriptions earlier in this section. Similar to the specimens from Series 1, the punching shear failure is best illustrated through the load-deflection curve in Figure 32. The load-deflection curve for a flexural failure, shown in Figure 33, illustrates the ability of the Ductal® slabs to hold a peak load through a slight increase in displacement, then support a reduced load while continuing to deform beyond the peak load.

The strain response was observed to be similar in nature regardless of failure mode and primarily dependent on the location of the strain gauge placement relative to the crack formation pattern. Representative load-strain responses for Series 2 are illustrated in Figures 34, 35, and 36 for the diagonal, orthogonal, and loading face locations, respectively. The limiting strain for a 2.5 in thick slab is 7090με.

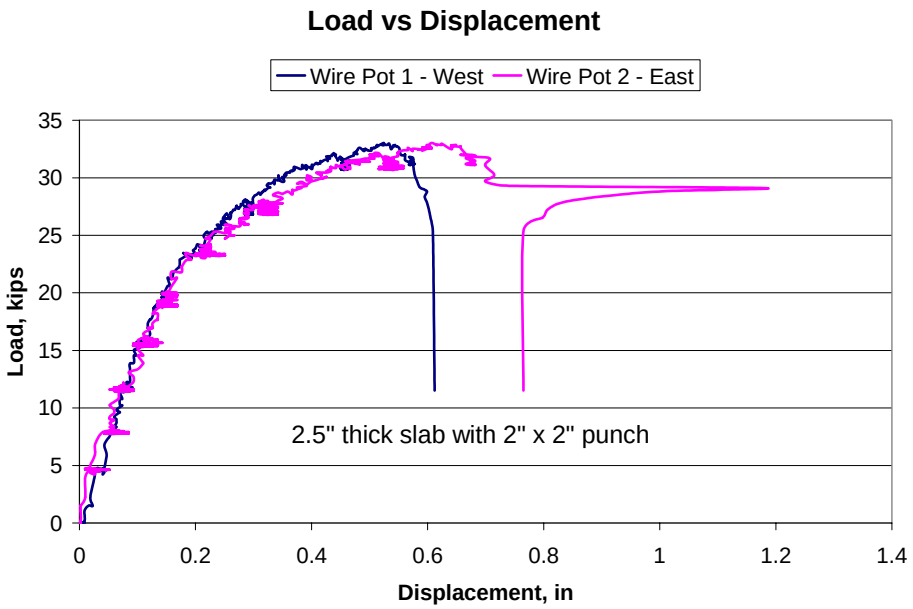

Figure 32. Typical Load vs. Displacement Curve for Series 2 – Slab #1 (Punching Shear Failure)

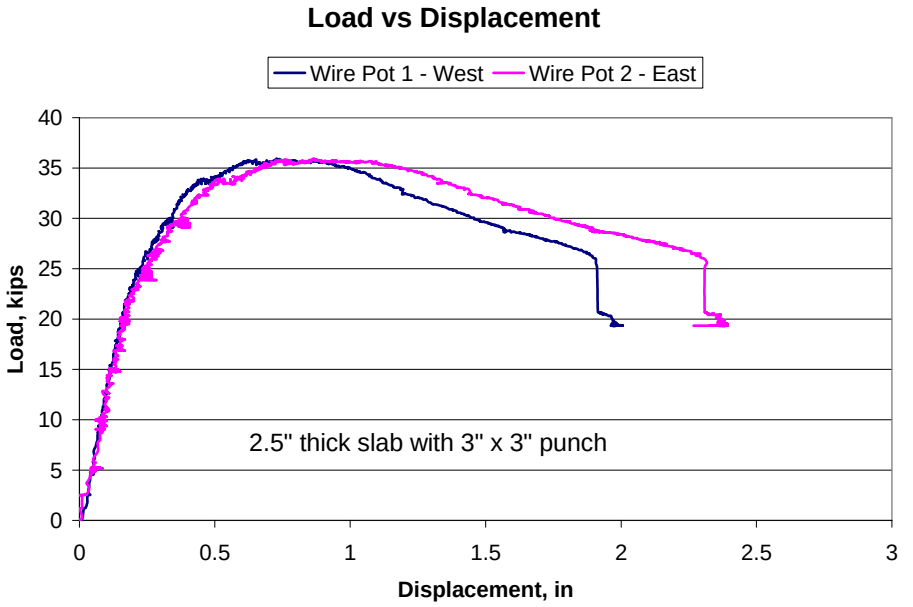

Figure 33. Typical Load vs. Displacement Curve for Series 2 – Slab #2 (Flexural Failure)

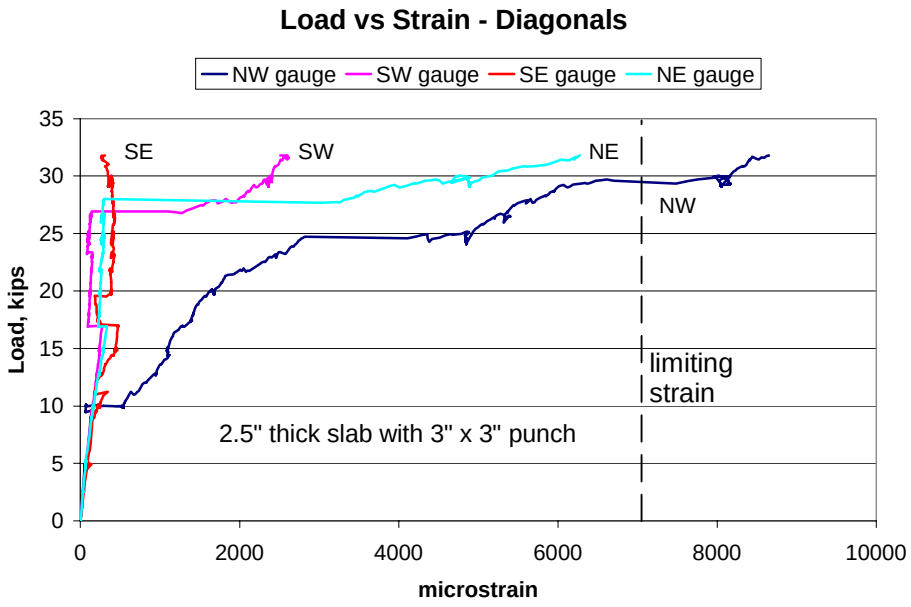

Figure 34. Typical Load vs. Strain for Gauges on Diagonals for Series 2 – Slab #2 (Tensile Face)

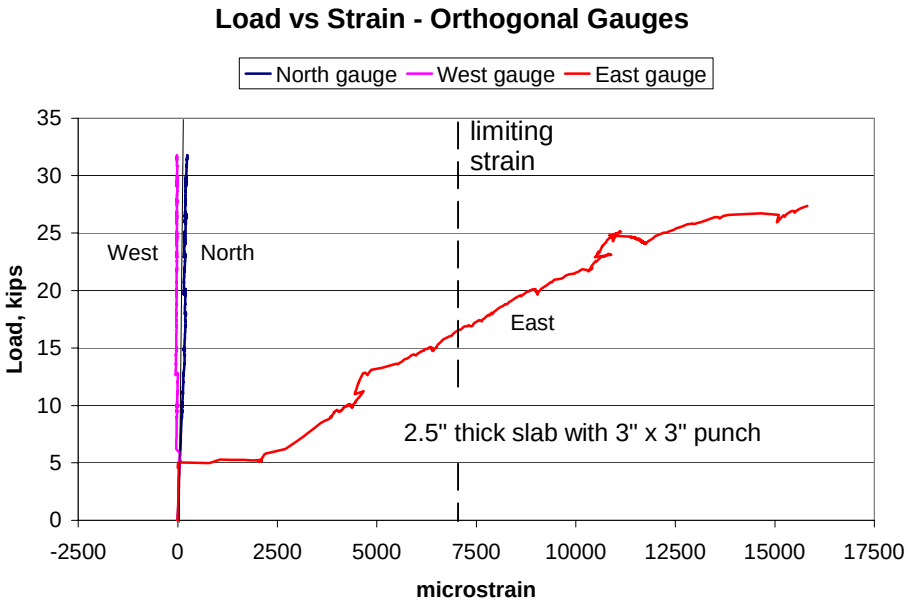

Figure 35. Typical Load vs. Strain (Orthogonal) for Series 2 – Slab #2 (Tensile Face)

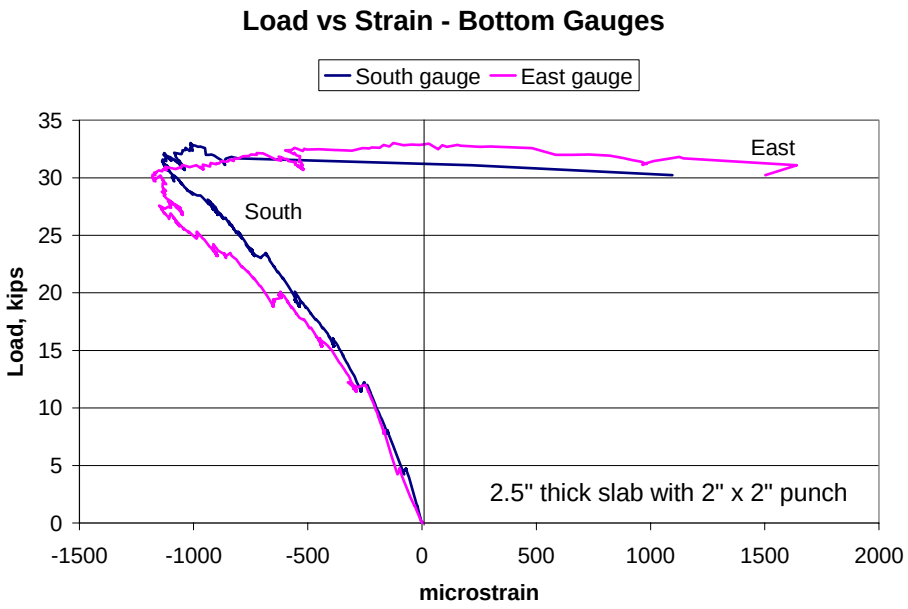

Figure 36. Typical Load vs. Strain (Loading Face) for Series 2 – Slab #1

As was the case with the slabs from Series 1, the slabs tested in Series 2 experienced an increase in failure load as the punch plate dimensions increased, but failed to accurately match the predicted response as seen in Table 10. In both the flexural and punching shear failure, the predicted failure loads were higher than the actual failure loads.

Series 3 Results

The slabs tested in Series 3 were all approximately 3.0 in thick specimens. In Series 3, a total of five slabs were tested; the fifth slab tested was originally intended to be cast as a 2.0 in slab, but was poured in excess and was measured to be approximately 3.0 in over the unsupported region. The results from Series 3 are shown in Table 11.

Table 11. Series 3 Test Results

			Predicted			Actual		
Test No.	**Slab Thickness in**	**Punch Plate Size in**	**Punching Failure Load kips**	**Flexural Failure Load kips**	**Failure Mechanism**	**Failure Mechanism**	**Failure Load kips**	**Average Maximum Deflection$_{(midspan)}$ in**
1	3.10	2.5	76.5	62.4	Flexural	Flexural	39.0	1.51
2	2.83	1.5	59.4	50.6	Flexural	Punching	35.2	0.60
3	3.03	1	52.8	56.8	Punching	Punching	40.1	1.08
4	2.85	2	66.0	52.2	Flexural	Flexural	38.4	1.66
5	3.27	1.75	63.0	67.5	Punching	Flexural	39.4	1.80

Similar to the results from the other series, a small plate was required to produce a punching shear failure. Additionally, the prediction equations were not as accurate in predicting the failure mechanism as in previous tests.

Similar to the specimens from Series 1 and 2, the punching shear and flexural failures are best illustrated through load-deflection curves (Figures 37 and 38). The punching shear failures in Series 3 differed from those in Series 1 and 2 in that the specimens were able to sustain a reduced load while continuing to deform, similar to a flexural failure. This indicates there was wide spread flexural cracking prior to the final punching failure. For the specimens of Series 3, the failure mechanisms were titled punching shear failures based on the abrupt conical failure during testing.

The load-strain responses for both the flexural and punching shear failures were similar for both failure types and of similar form to the responses observed in Series 1 and 2. Representative load-strain responses for Series 3 are illustrated in Figures 39, 40, and 41 for the diagonals, orthogonal, and loading face locations, respectively. The limiting strain for a 3 in thick slab is 5910με.

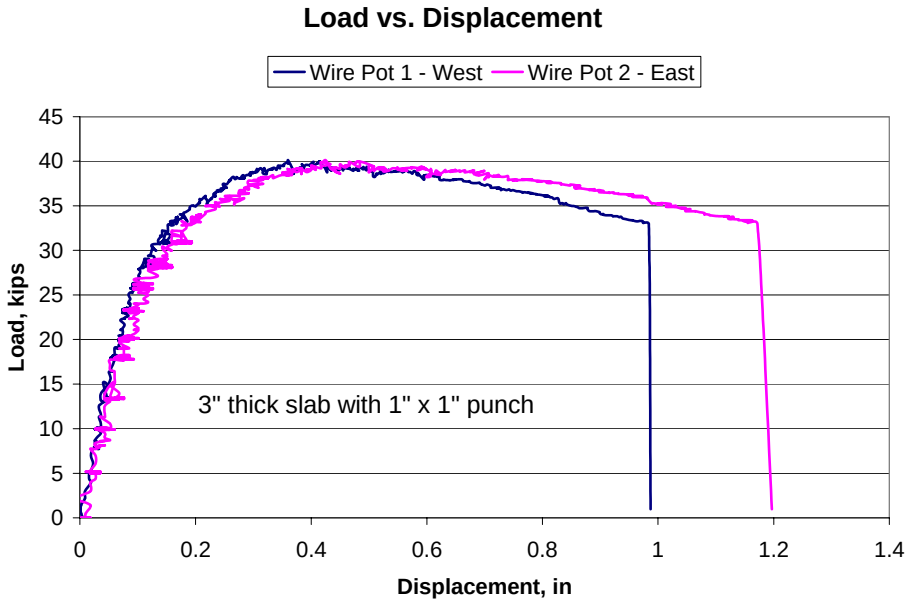

Figure 37. Typical Load vs. Displacement Curve for Series 3 – Slab #3 (Punching Shear Failure)

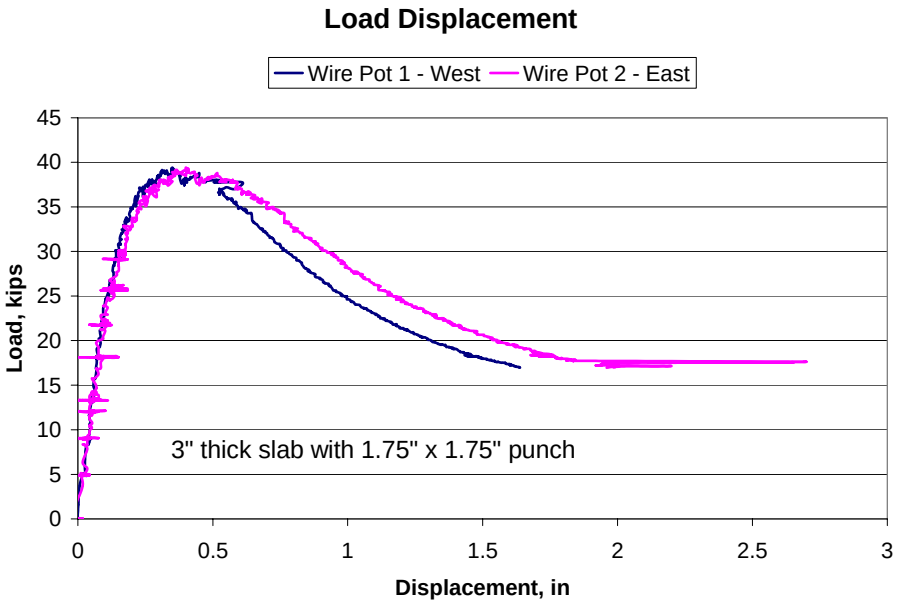

Figure 38. Typical Load vs. Displacement Curve for Series 3 – Slab #5 (Flexural Failure)

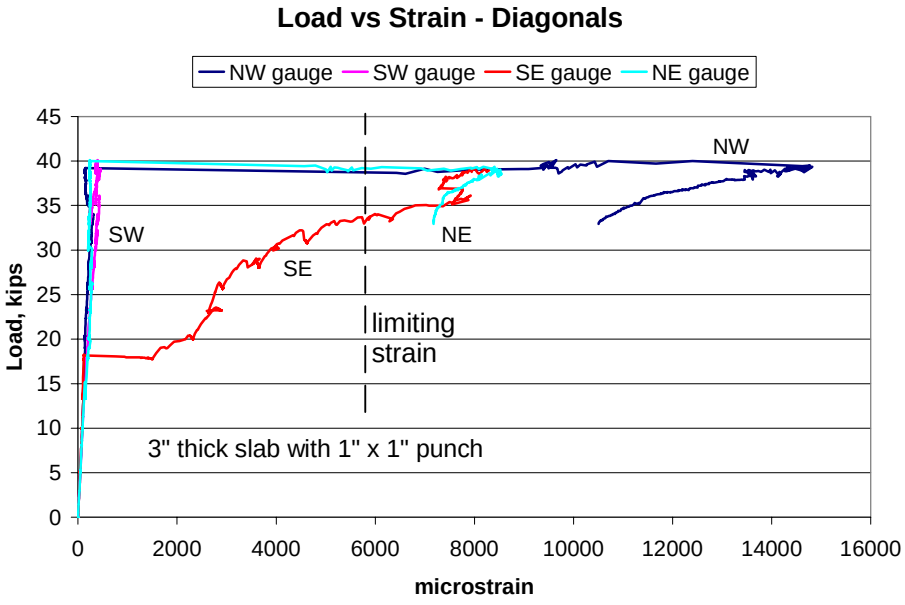

Figure 39. Typical Load vs. Strain for Gauges on Diagonals for Series 3 – Slab #3

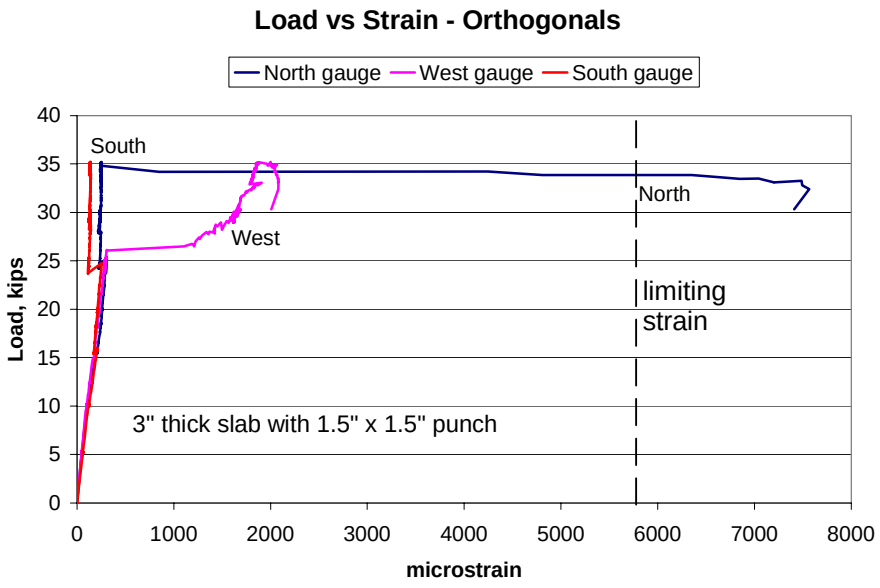

Figure 40. Typical Load vs. Strain (Orthogonal) for Series 3 - Slab #2

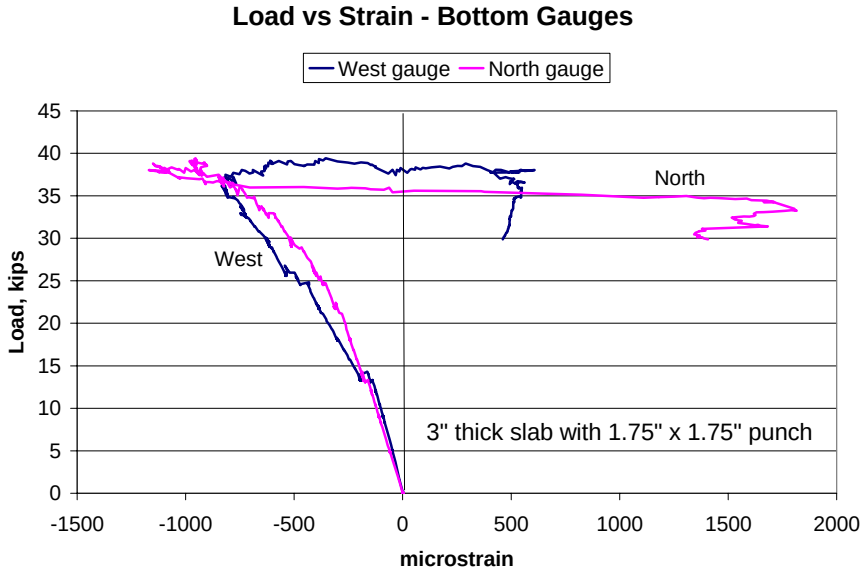

Figure 41. Typical Load vs. Strain (Loading Face) for Series 3 - Slab #5

Similar to results from Series 1 and 2, the slabs tested in Series 3 experienced an increase in failure load as the punch plate dimensions increased, but failed to accurately match the predicted response (Table 11). For both failure modes, the predicted failure loads were higher than the actual failure loads. Additionally, the predicted failure mechanism was not always in agreement with the actual failure mechanism.

Series 4 Results

As stated earlier, all of the large plate specimens exhibited flexural failures. Test results are presented in Table 12. Figure 42 presents a comparison of the load vs. mid-span deflection curves for the three specimens. Slabs 1 and 2 were similar in thickness and in support conditions. Slab 1 was approximately 9% thicker than Slab 1, but was able to support a peak load 22% higher than Slab 2. It could be a reflection of the inherent variability in the material, or a reflection of the overall average thickness of the slab, which was difficult to accurately determine. It also could be variability in the actual support conditions. The edges were restrained between the frame and a channel, and bolts, on 9 in centers, were tightened. Due to misplaced bolt holes and other slab variabilities, the support conditions of the two slabs may not have been equivalent. Slab 3, which was pinned at the edges, achieved a much lower peak load compared to Slabs 1 and 2, as would be expected because of the boundary conditions and the smaller average thickness.

Figures 43, 44 and 45 present typical load versus strain plots for strain gauges that were located at or near the locations of cracks. The top and bottom strains were very similar prior to cracking, as would be expected. At a load of 5 kips, the slabs were all exhibiting similar strains of around 50 to 70 με. None of the measured strains in these tests approached the limiting strains for the respective slab depths.

Table 12. Results of Series 4 – Large Slabs

Slab No.	Average Slab Thickness, in	Cracking Load, kips	Maximum Load, kips	Deflection at Max. Load, in
1	3.05	9.5	27.9	1.06
2	2.80	8.5	22.9	2.6
3	2.70	6.3	14.7	1.41

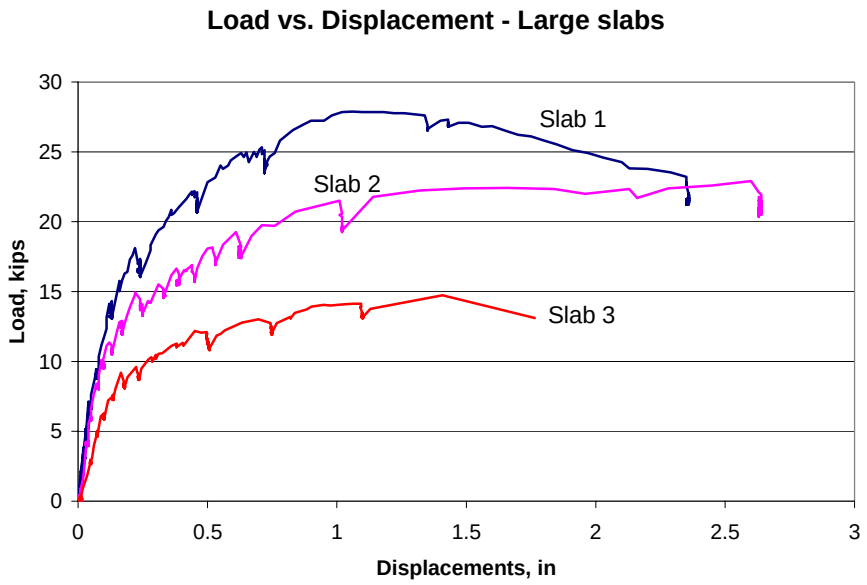

Figure 42. Load vs. Deflection Plots for Series 4 Slabs

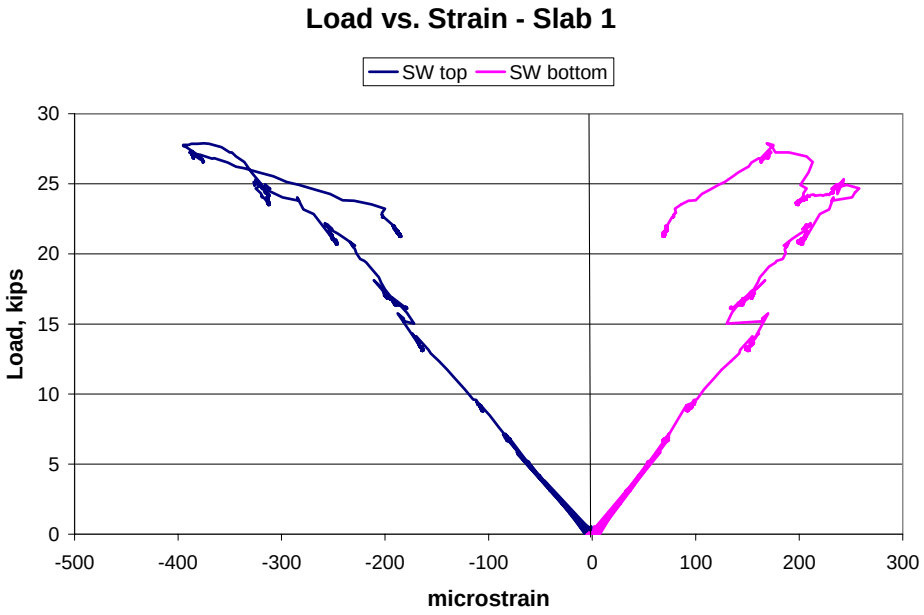

Figure 43. Typical Load vs. Strain Plot for Gauges on Slab 1 in Series 4.

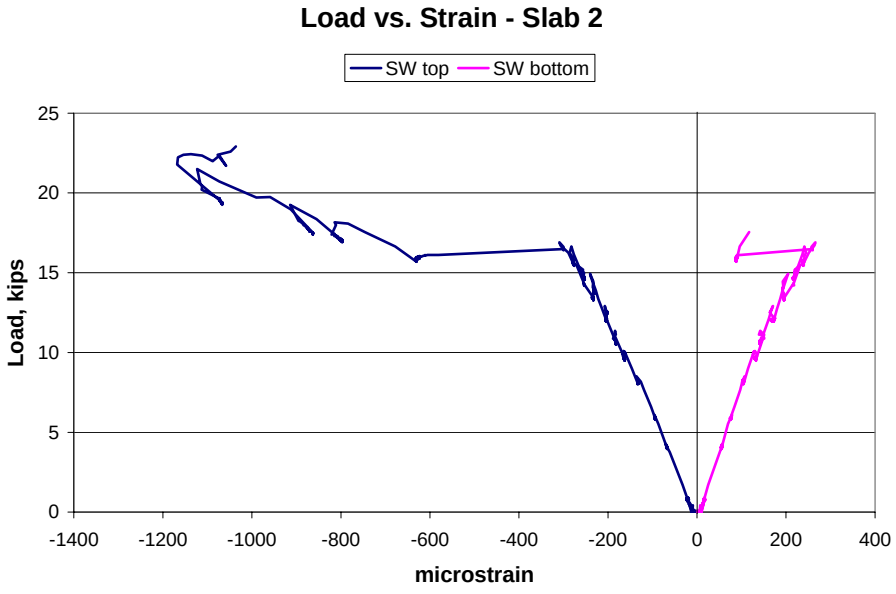

Figure 44. Typical Load vs. Strain Plot for Gauges in Slab 2 of Series 4.

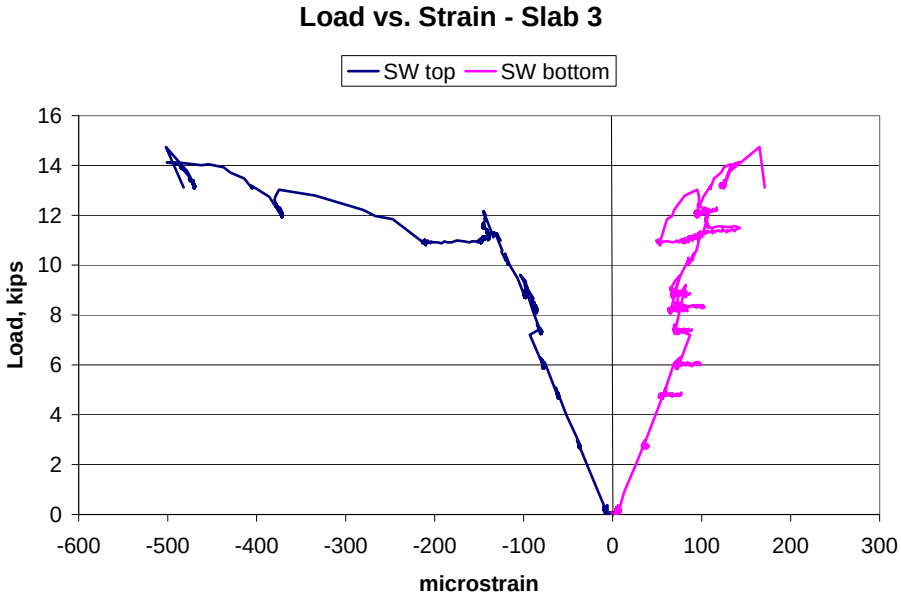

Figure 45. Typical Load vs. Strain Plot for Gauges in Slab 3 of Series 4

Punching Shear Strength Prediction Models

In this section a series of models and equations are presented and compared to the results obtained during testing. Some of the equations presented are from other researchers' studies of punching shear, others are models from derived from the ACI 318-02 Code (2002), and the last are equations modeled to fit the results using curve fitting software. The models are first presented in this section, then compared to results.

Narayanan and Darwish Equation

Narayanan and Darwish (1987) studied the effect of steel fiber reinforcement on the punching shear capacity of micro-concrete slabs by testing twelve simply supported slabs to failure. The parameters considered in the study were volume fraction of fibers, amount of tensile reinforcement, and concrete strength. The results indicated that an increase in fiber content improved the shear strength and modified the position of the critical perimeter. The authors proposed that the design of concrete slabs for shear can be similar to that for beams and suggested the following equation for the prediction of punching shear

$$v_u = \xi_s \left(A' f_{spf} + B'' \rho + v_b \right) \quad \text{MPa} \tag{3}$$

where:

ξ_s = empirical depth factor
A' = non dimensional constant = 0.24
f_{spf} = split cylinder strength of fiber reinforced concrete (MPa)
B" = dimensional constant = 16
ρ = area percent of tensile steel reinforcement (%)
v_b = vertical fiber pull-out stress along inclined crack (MPa)

The equation proposed by Narayanan and Darwish (1987) was further expanded by Tan and Paramasivam (1994) as

$$v_u = \frac{P_u}{\xi_s u_b d} = 0.24 f_{sp} + 16\rho + 0.41\tau_u \rho_f d_f \frac{L}{D} \qquad \text{MPa} \qquad (4)$$

where:

u_b = critical perimeter = $(1 - 0.55 \cdot \rho_f \cdot d_f \cdot \frac{L}{D}) \cdot (4 \cdot r + 3 \cdot \pi \cdot h)$
h = slab thickness (mm)
r = width of loading platen (mm)
d = average effective depth to tension reinforcement (mm)
ξ_s = empirical depth factor = $(1.6 - 0.002 \cdot h)$
f_{sp} = split cylinder strength of fiber reinforced concrete (MPa)
ρ = area percent of tensile steel reinforcement (%)
τ_u = average fiber matrix interfacial bond stress = 4.15 MPa
ρ_f = volume fraction of steel fibers (%)
d_f = factor for fiber type = 0.5 (round), 0.75 (crimped), 1.0 (duoform-steel fibers)
L = length of fibers (mm)
D = diameter of fibers (mm)

In the form proposed by Tan and Paramasivam (1994), the contribution by the concrete (term 1), the tensile reinforcement (term 2), and the steel fibers (term 3) can be distinguished. In order to use this equation, the term that represents the tensile steel contribution was excluded because no tensile reinforcement was used in the Ductal® slabs tested. The final equation form is:

$$v_u = \frac{P_u}{\xi_s u_b d} = 0.24 f_{sp} + 0.41\tau_u \rho_f d_f \frac{L}{D} \qquad \text{MPa} \qquad (5)$$

Shaaban and Gesund Equation

Shaaban and Gesund (1994) studied the effects of steel fibers on the punching shear strength of reinforced concrete slabs (flat plates), specifically whether the addition of steel fibers significantly enhanced the punching shear capacity. Thirteen slabs with varying fiber contents were tested to failure and produced results that demonstrated the enhancement in punching shear capacity achieved with the addition of fibers. The authors proposed an equation of the same form as the ACI 318-02 Code (2002) equation for punching shear, but modified it to account for the fiber contribution. The equation proposed is:

$$V_c = \left[(0.3 W_f + 6.8) \frac{\sqrt{f'_c}}{1000} \right] b_o d \qquad \text{kips} \qquad (6)$$

where: W_f = percent of fibers by weight of concrete (%)
f'_c = concrete compressive strength (psi)
b_o = critical perimeter as defined by ACI (in)
d = average effective depth to tension reinforcement (in)

The advantage of this equation is that it maintains the general form of the ACI 318-02 code equations for punching shear. However, in the testing performed in the current research effort the percent of fibers by weight of concrete (W_f) was not varied. A standard 2% by volume was used in all slabs. Therefore, it is difficult to evaluate the applicability of this term to the tested slabs.

Modified ACI Equation for Concrete Breakout Strength

Observations were made of the failure surface of the test specimens and it was concluded that the conical failure was similar in appearance to the breakout cone for concrete as shown in ACI 318-02 (2002) for a surface with an embedded bolt in tension (Figure 46). The only significant difference observed was that in the ACI 318-02 code the size of the bolt head has no impact on the failure cone. The equation proposed by the ACI 318-02 Code is:

$$N_b = k\frac{\sqrt{f'_c}}{1000}h_{ef}^{1.5} \qquad \text{kips} \tag{7}$$

where: N_b = basic concrete breakout strength in tension for single anchor in cracked concrete (kips)
k = coefficient for basic concrete breakout strength in tension
= 24 (cast-in anchors)
= 17 (post-installed anchors)
f'_c = concrete compressive strength (psi)
h_{ef} = effective anchor embedment depth (in)

Modifications were made to this equation to predict the strength of Ductal® subjected to a tensile load; this tensile load was assumed to be equivalent to the applied punching load. Similar to the bolt head applying load to the slab through the head, the load is applied to the Ductal® slabs by the loading plate as seen in Figure 44.

A post failure survey of the slabs was made to investigate the failure surface angle. Although the failure surfaces were most often rectangular or oblong, rather than square or circular, the average side length was approximately equal to 3 times the slab depth plus the loading plate dimension. This matches well the concrete breakout failure surface shown in Figure 44.

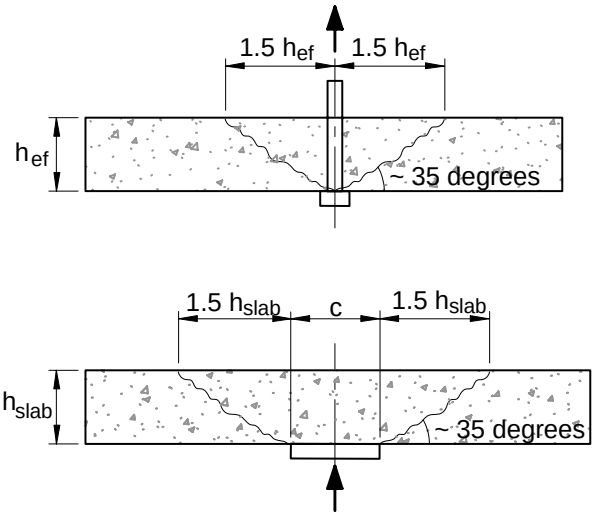

Figure 46. Concrete Breakout and Punching Shear Failure Surfaces

For concrete breakout strength, the ACI 318-02 code refers to the work of Fuchs et al. (1995), which states that the concrete conical failure depends on the tensile capacity of the concrete, considered to be proportional $\sqrt{f'_c}$. With the increased tensile capacity achieved with Ductal®, it would be expected that an increase in the concrete breakout strength could be achieved. The proposed equation based on the work by Fuchs et al. (1995) is:

$$V_c = N_b = k_1 f_t \frac{(3h + c)^2 - c^2}{\sqrt{h}} \qquad \text{kips} \tag{8}$$

where:
- f_t = split cylinder tensile strength (ksi)
- k_1 = empirical constant
- h = slab thickness (in)
- c = loading plate dimension (in)

The proposed equation reduces to the original ACI equation as ***c*** approaches zero. The significant difference between the original ACI equation for concrete breakout strength and the modified equation is the consideration of the bolt head and loading plate area. The ACI equation does not consider the area of the bolt head in the conical failure surface, while the plate area is considered in the modified equation. This equation was compared to the test results and a curve fitting software (NLREG 2004) was used to determine the value of the empirical constant k_1. It was determined to be 0.38.

ACI Curve – Fit Equations

Empirical equations, historically, have served as the foundation for the ACI prediction of punching shear capacity; the equations were developed based on test data with little emphasis placed on a model to characterize the true failure mechanism (ASCE-ACI Task Committee 1974). The use of these empirically developed equations has continued over the years with only minor changes, but the general form is still maintained. This illustrates that the use of empirical

equations is not uncommon, but the trend in recent years has been to develop empirical equations that maintain the same general form of the ACI 318-02 design equations. This was the method used in the preliminary analysis.

Using a nonlinear regression and curve fitting software package (NLREG), numerous iterations were performed to fit an equation similar in form to the ACI design equations for punching shear to the test data for the UHPC slabs. The general form of the equation developed is:

$$V_c = k_3 \cdot f_t \cdot b_o \cdot d_{equiv} \text{ (kips)} \quad (9)$$

where:
- k_3 = empirical constant relating tensile strength to compressive strength = 0.02 (from curve fitting)
- f_t = split cylinder tensile strength (ksi)
- b_o = critical perimeter = $4 \cdot (c + a \cdot h + M)$ (in)
- c = loading plate side dimension (in)
- h = slab thickness (in)
- d_{equiv} = equivalent effective depth = a x h (in)
- a = empirical factor relating slab thickness to equivalent effective depth = 5.29 (from curve fitting)
- M = empirical constant (assumed to represent the fiber contribution to the critical perimeter) = 7.81 (in) (from curve fitting)

This empirical equation was derived with the ACI design equations for punching shear capacity as the foundation, but was modified to provide a reasonable fit to the test results. However, these modifications left some uncertainty in the interpretation of the model. The empirical factor M cannot be physically defined for the critical perimeter. It is assumed that this empirical factor, M, represents the contribution of the fibers to an increase in the critical perimeter, but based on the limited test data this cannot be verified. Also the factor k_3, which should represent the effective tensile strength of the concrete on the failure surface, is very small, while a, which represents the portion of the slab depth effective in resisting punching shear, is very large. These irregularities make the applicability of the equation to situations beyond the boundaries of the test series questionable.

Comparison of Results to Model Equations

In general the various models previously discussed performed well when compared to the results of the tests. Most of the established models provided a reasonable representation of the response. Note that in the figures only the seven slabs that were deemed to have failed in punching shear are presented.

Preliminary Analysis

The equation derived during the preliminary analysis overestimated the punching shear capacity of the test slabs. As illustrated in Figure 47, the predictions are consistently unconservative with all of the predicted failure loads exceeding the measured capacities. The results from this equation could be factored down to better match the measured data, which would indicate that the tensile capacity is not being fully utilized. Additionally, the predicted capacity was calculated based on the tensile capacity ($f_t + k_m = 0.1 + 1.0$ ksi) proposed by Park et al. (2003) which was lower than the tensile capacity measured from the split cylinder tests conducted by Graybeal (2004) which ranged from 1.5 – 1.7 ksi. Using the actual tensile capacity makes the prediction more unconservative. The lack of full tensile capacity could be attributed to the fiber orientation that did not appear to be as random as expected. Random orientation was likely not achieved due to the thinness of the slab, which did not allow for orientation of the fibers perpendicular to the formed surface. This differs significantly from the tensile test specimens where the fibers are randomly oriented.

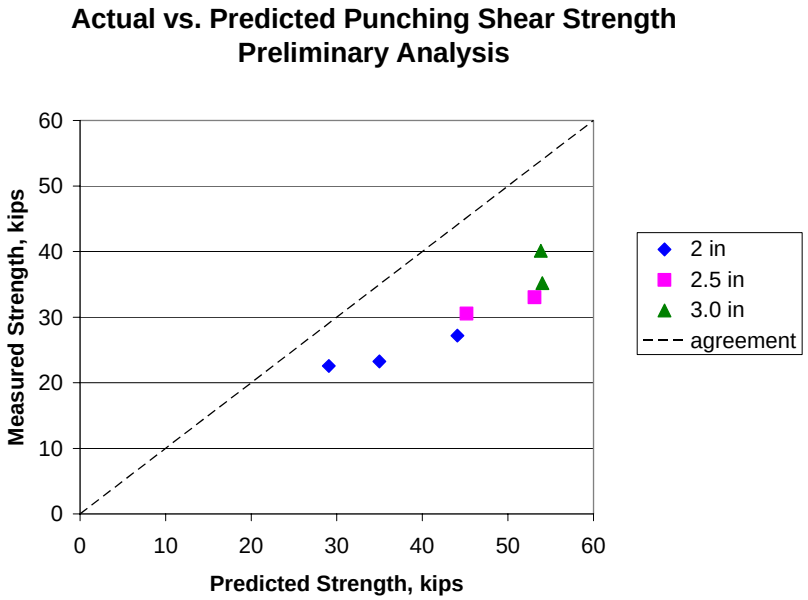

Figure 47. Preliminary Analysis Prediction for Punching Shear Capacity vs. Actual

ACI Punching Shear Design Equation

The ACI 318-02 punching shear equation (ACI 318, 2002) is presented as Equation 1, and is restated below:

$$V_n = 4\sqrt{f'_c}(c+h)4h \qquad (1)$$

This equation resulted in a better prediction of the punching shear capacity than the preliminary analysis equation as illustrated in Figure 48. The only alteration to the ACI equation was that the effective depth of the tensile reinforcement was replaced with the slab thickness because no tensile reinforcement was used in the test slabs. For the UHPC used in this research,

$4 \cdot \sqrt{f'_c}$ equates to 714 psi, which is slightly less than half of the measured splitting tensile strength of 1.6 ksi.

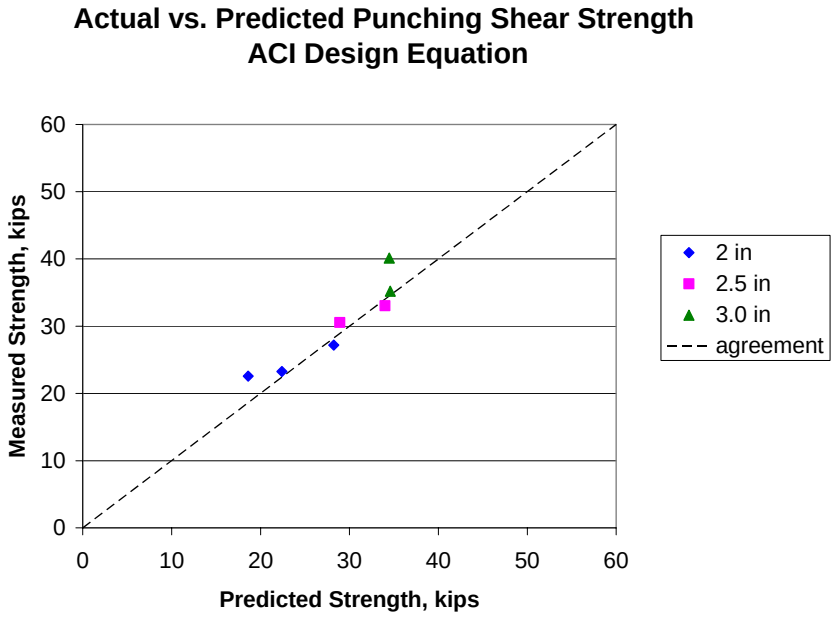

Figure 48. ACI 318-02 Prediction for Punching Shear Capacity vs. Actual

Narayanan and Darwish Equation

The equation proposed by Narayanan and Darwish (1987) provided a reasonable prediction for some of the test slabs, specifically the 2.0 in slabs, but was unconservative for the other thicknesses. The comparison is illustrated in Figure 49.

Shaaban and Gesund Equation

The equation proposed by Shaaban and Gesund (1994) provided a rather unconservative prediction of punching shear strength (Figure 50). The difficulty in properly evaluating this equation is that one of the premises on which the equation is based is that the fiber content is a factor in the punching shear capacity prediction and for this experiment the fiber content was not varied.

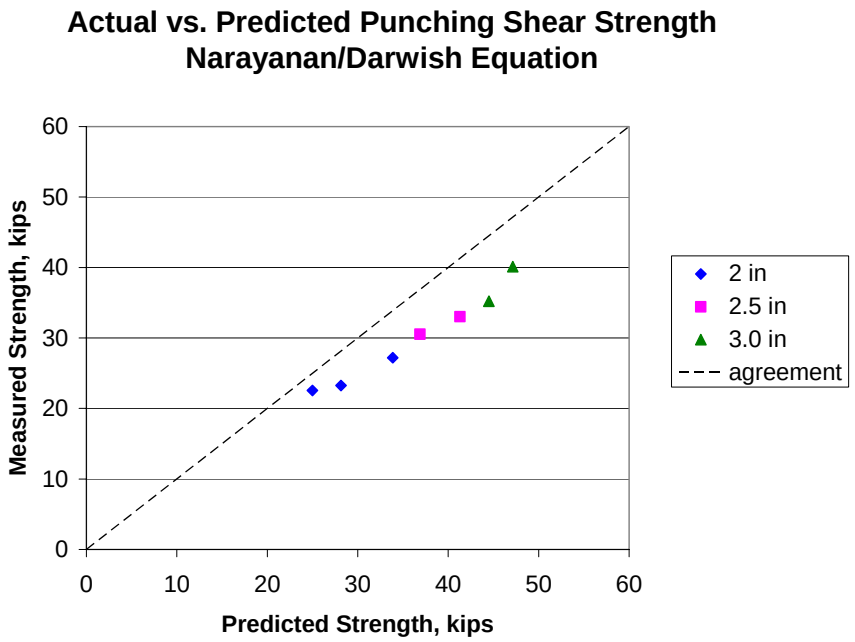

Figure 49. Narayanan & Darwish Prediction for Punching Shear Capacity vs. Actual

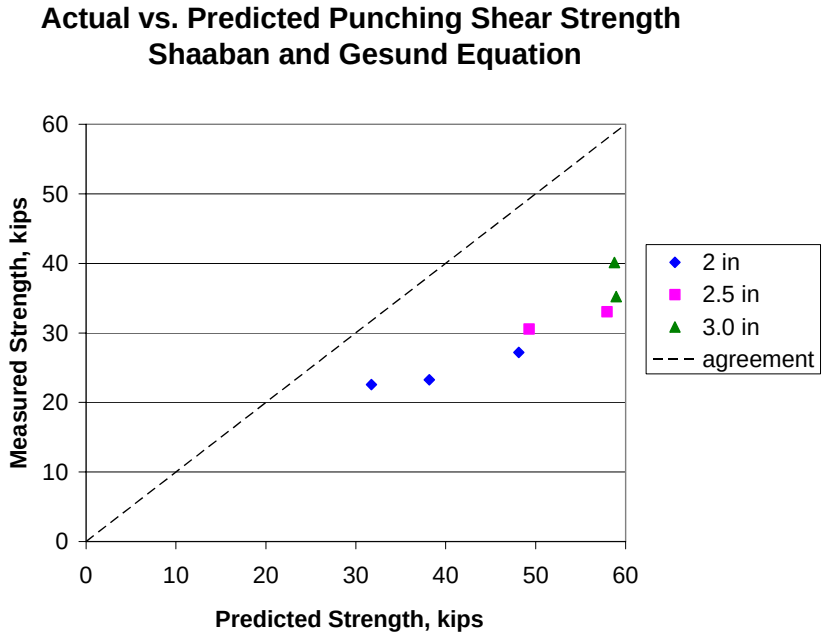

Figure 50. Shaaban & Gesund Prediction for Punching Shear Capacity vs. Actual

ACI Concrete Breakout Equation

The equation for concrete breakout strength from the current ACI 318-02 Code (2002) is not considered to be an equation for the punching shear capacity of concrete, but the failure mechanisms are similar. The modified equation was presented previously as Equation (8). As illustrated in Figure 51, this equation provides a good prediction of the punching shear capacity,

but this is as a result of the empirical constant being derived from curve-fitting using NLREG. A similar trend could be observed in the original ACI prediction equation if a curve fit were used to improve the fit of the curve to the data (i.e., modifications made to the constant relating compressive strength to tensile strength).

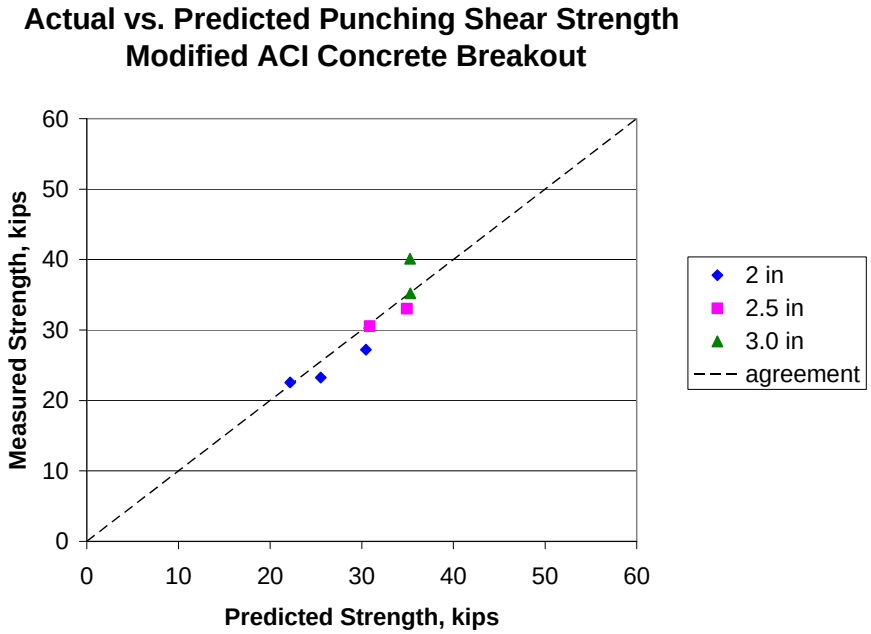

Figure 51. Modified ACI Prediction for Concrete Breakout (Punching) Capacity vs. Actual

ACI Curve-Fit Equation

As would be expected with any curve fit equation, the predictions match the test results very well. The curve fit was based on the general form of the ACI 318-02 punching shear equation with terms for the tensile capacity, critical perimeter, and effective depth adjusted to provide the best fit to the data set. The difficulty that arises from using this equation is the limited number of data points to develop the curve and the unknown interpretation of the empirical constants **M, k_3** and **a** (Equation 9). The performance of the equation is illustrated in Figure 52.

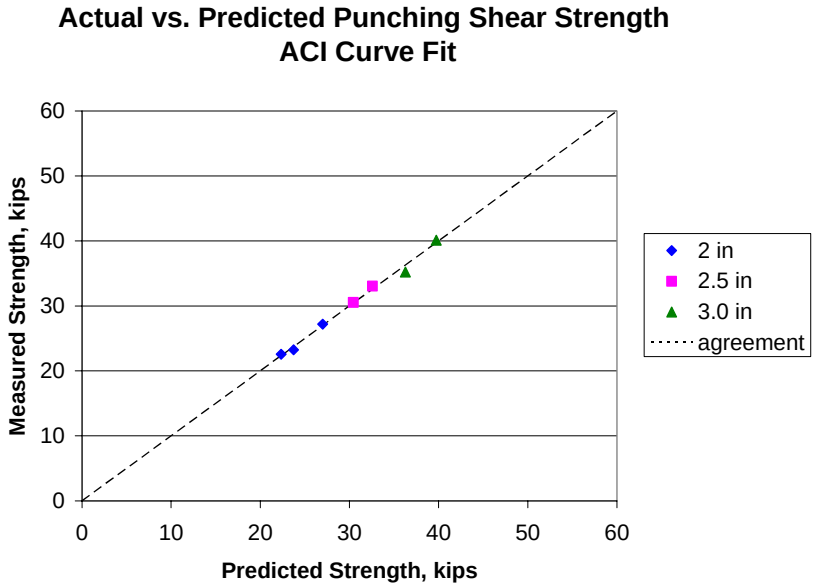

Figure 52. Curve-Fit Prediction for Punching Shear Capacity vs. Actual

Comparison of Prediction Equations

Each of the presented equations provides some advantages and disadvantages, but all tend to provide a reasonably consistent measure of the response. The prediction methods were compared statistically to determine the best predictor. Although the data set is limited, there is not a significant amount of scatter in the data and the use of statistical comparisons should provide a good measure of the relative effectiveness of each equation. A statistical analysis of the measured response to the predicted response is provided in Table 13.

Table 13. Statistical Results

			Prediction Equation					
			Preliminary Analysis	ACI	Narayanan/ Darwish	Shaaban/ Gesund	Modified Concrete Breakout	Curve Fit
Slab Thickness in	Punch Size in	Actual Load kips	V_{act}/V_{cal}	V_{act}/V_{cal}	V_{act}/V_{cal}	V_{act}/V_{cal}	V_{act}/V_{cal}	V_{act}/V_{cal}
2.12	1	22.6	0.78	1.21	0.90	0.71	1.03	1.01
2.17	1.5	23.3	0.66	1.04	0.83	0.61	0.92	0.98
2.32	2	27.2	0.62	0.96	0.80	0.57	0.90	1.01
2.54	1.5	30.5	0.68	1.06	0.83	0.62	1.00	1.00
2.61	2	33.0	0.62	0.97	0.80	0.57	0.95	1.01
3.03	1	40.1	0.75	1.16	0.85	0.68	1.15	1.01
2.83	1.5	35.2	0.65	1.02	0.79	0.60	1.01	0.97
Mean			**0.68**	**1.06**	**0.83**	**0.62**	**0.99**	**1.00**
Standard Deviation			**0.06**	**0.09**	**0.04**	**0.06**	**0.08**	**0.02**
Coefficient of Variation			**8.9%**	**8.9%**	**4.6%**	**8.9%**	**8.3%**	**1.7%**

Several of the models provided reasonable estimates for the prediction of punching shear capacity of UHPC. The results illustrate that the range of the mean of the measured load to the predicted load ranges from 0.62 – 1.06 while the coefficient of variation only ranges from 1.7 – 8.9%, excellent agreement for a cementitious material. This agreement is likely achieved due to the uniformity of UHPC resulting from the controlled batching environment and the lack of coarse aggregate, which could reduce the uniformity. The results of the analysis indicate that the best model for predicting the punching shear capacity is the *Curve Fit Equation* as should be expected, but as previously stated there is some uncertainty in the defined critical perimeter and this equation will not be recommended for design. The next model considered was the *Modified Concrete Breakout Equation* due to its mean being very close to 1.0 and its low coefficient of variation. For these reasons, the *Modified Concrete Breakout Equation* will be considered the best model for the prediction of the punching shear capacity of UHPC slabs. The current *ACI 318-02 Code Equation* (ACI 2002) could also be used; the mean is slightly more conservative and the coefficient of variation is slightly higher, indicating more scatter around the mean. Both equations were very good predictors of punching shear strength.

Flexural Failures

While the purpose of this research was to develop a prediction measure of the punching shear capacity of UHPC, a number of flexural failures occurred during the testing and these are also examined. The sole method used to predict the flexural capacity of UHPC was yield line analysis, which serves as an upper bound analysis technique. The results of the Ductal® flexural failures did not exhibit good agreement with the predictions from yield line analysis as illustrated in Figure 53. Yield line analysis overestimated the flexural capacity of Ductal® slabs in all tests and all cases by a significant amount as shown in Table 14. The disagreement with the prediction model can likely be attributed to two main factors; the difference in flexural capacity between orthogonal directions caused by the fibers not being randomly oriented, and the material not being ideal for use of yield line analysis based on moment-curvature relationships observed. Another possible source of disagreement is the boundary conditions. It was assumed that the edges were fully fixed, but if some rotation were allowed, the failure load would be reduced. Further analysis of the flexural capacity is required to gain a better understanding of the behavior, but this is beyond the scope of this research effort.

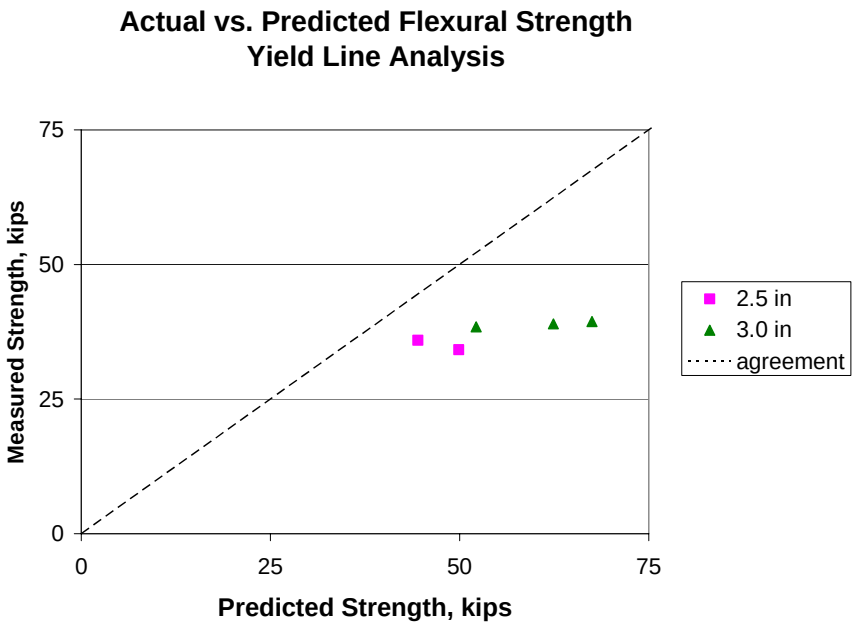

Figure 53 – Yield Line Analysis Prediction for Flexural Capacity vs. Actual

Table 14. Summary of Flexural Failure Results

Slab Thickness in	Punch Dimension in	Actual Failure Load kips	Predicted Failure Load kips	Actual/ Predicted
2.58	3	35.9	44.5	0.81
2.76	2.5	34.2	49.9	0.69
3.10	2.5	39.0	62.4	0.63
2.85	2	38.4	52.2	0.74
3.27	1.75	39.4	67.5	0.58

Table 15 presents the actual loads compared to the loads predicted using yield line theory for the large slabs. All of the large slabs were also flexural failures. Both fully fixed and pinned edge conditions were investigated. For analysis it was assumed that the flexural strength in all directions was equal. As can be seen from the results, the method significantly underpredicts actual strength, particularly for the restrained slabs.

Table 15. Results of Series 4 slabs compared to predictions

Slab No.	Average Slab Thickness in	Actual Failure Load, kips	Calculated M_n per unit Length in-k/ft	Predicted load with pinned edges, kips	Predicted load with fixed edges, kips	Actual/ Predicted
1	3.05	27.9	53.24	-	66.8	0.42
2	2.80	22.9	45.13	-	66.8	0.34
3	2.70	14.7	42.07	33.4	-	0.44

Proposed Slab Thickness

The results of the optimized section modeling performed by Park et al. (2003) suggested that the minimum slab thickness to be used in bridge applications is 4.0 in. This prediction was based on the no cracking Service Limit State (SLS) criterion proposed by the French Association of Civil Engineering (AFGC, 2003), which did not allow for any cracking to occur. Based on the results of the testing conducted, this criterion may be unrealistic because the load that caused cracking was significantly lower than the final failure load. The load to cause first cracking for the small slabs ranged from ~ 5 – 15 kips (presented in the Appendix) depending on the specimen thickness and the loading plate area. These cracking loads were significantly lower than the peak loads that ranged from 22.6 – 40.1 kips. For the large slabs, the cracking loads were 9.5, 8.5, and 6.3 kips while the ultimate loads were 27.9, 22.9, and 14.7 kips, respectively. This illustrates that the SLS criterion may be somewhat conservative for UHPC slab systems, since the ratio between ultimate load and first cracking load was over 2.0 for all cases. However, until the fatigue behavior of cracked UHPC is better understood, the no crack criterion is prudent.

Based on the results obtained from the testing, a very small loading plate is required in order to produce a punching shear failure prior to a flexural failure. The load that is applied to a bridge deck by the AASHTO HL-93 truck (16 kips per tire) or the Tandem truck (12.5 kips per tire) in design is distributed over an area of 8 in x 20 in (AASHTO, 2003). Based on the two best equations a minimum slab depth to prevent a punching shear failure can be determined. The two equations are shown below, and the punching shear strengths of 1 in and 2 in thick slabs are presented in Table 16.

$$V_c = 0.38 \cdot f_t \cdot \frac{(3 \cdot h + a) \cdot (3 \cdot h + b) - a \cdot b}{\sqrt{h}} \tag{8}$$

where *a* and *b* are the dimensions of the loading plate

$$V_c = 4\sqrt{f'_c}\, b_o h \tag{1}$$

where $b_o = 2a + 2b + 4h$

Table 16. Punching Shear Strength of Thin Slabs Loaded through Tire Patch

Slab Thickness, in	Load plus Impact Factor times load Factor, kips	Wheel Patch Dimensions in x in	Punching Shear Strength with Equation 8, kips	Punching Shear Strength with Equation 1, kips
1	37.2	8 x 20	56.4	42.9
2	37.2	8 x 20	87.7	91.4

The predicted nominal strengths in Table 16 are larger than the factored wheel patch load. Even with the AASHTO LRFD strength reduction factor for shear of 0.9, the 1 in thick slab would not fail in punching shear due to the factored wheel patch load. However, the slab thicknesses presented in the table are extremely small, far thinner than would ever be considered for the top flange of the optimized double-tee. The results of the large slab tests indicate that the critical failure mode for the top flange will most likely be transverse bending rather than punching shear.

Summary of Results

The punching shear strengths were well predicted by two equations: the Modified Concrete Breakout Equation derived from the ACI 318-02 Code equation for concrete breakout resulting from a bolt anchored in concrete (Equation 8), and the original ACI punching shear strength equation (Equation 1). The limited number of data points makes the statistical analysis questionable, but the minimal variance leads to the assumption that the equations are sufficiently accurate for design purposes. It should also be noted that the results do not take into consideration the effects of axial loads on the slab systems, which would be the case for a prestressed system as proposed by Park et al. (2003). The addition of prestressing in the slab system could significantly change the stress distribution in the slab, which might alter the punching shear capacity. Further analysis would be required to verify the effects of prestressing, but it is beyond the scope of this research project. All large slabs failed in flexure at loads well below predicted values.

CONCLUSIONS

The following conclusions are made based on the test results and analysis:

- In the small plate tests, a very small loading area was required to force a punching shear failure in the UHPC slabs. Based on this assessment, a 1.0 in slab thickness should provide sufficient punching shear capacity for bridge applications. The actual slab thickness selected for design should also consider factors such as web spacing, preventing cracking at service load levels, flexural capacity, and deflection criteria.

- The modified ACI equation for concrete breakout strength provides the best measure of the punching shear capacity of UHPC slabs. The equation is as follows:

$$V_c = N_b = 0.38 \cdot f_t \cdot \frac{(3 \cdot h + c)^2 - c^2}{\sqrt{h}} \tag{8}$$

- The original ACI 318 equation for punching shear also predicted failure loads reasonably well. This equation is as follows:

$$V_n = 4\sqrt{f'_c}\,(c + h)4h \tag{1}$$

- For slab depths greater than the 3 in tested in this research program, Equation 8, because it considers size effects, will provide more conservative predictions of punching shear strength than Equation (1).

- The limiting strain criterion proposed in the MIT Report (Park et al. 2003) should be followed due to the lack of consistent data from the testing. The measured strains were highly dependent on the location of crack formation.

- Fibers tend to align in the direction of the flow of the material and also with the formwork; this may result in different flexural capacities in different directions.

RECOMMENDATIONS

1. UHPC slabs should be designed for punching shear based on Equation (8).

2. For flexural design, the top flange of the optimized double-tee should be designed to have no cracking under service loads. The resulting slab thickness should provide a factor of safety against failure of over 2.0 even if the fiber orientation is not as random as desired.

COST AND BENEFITS ASSESSMENT

Currently the cost of UHPC is quite high. The cost of the material has been quoted as being between $1,000 and $1,500 per cubic yard at the batch plant (Semioli 2001; Bonneau et al. 1996). This is considerably more than the cost of concrete, at around $100 per cubic yard, but much less than the cost of steel, which at around $0.60 per pound is almost $8,000 per cubic yard. Also, placement costs of UHPC should be less than those with conventional HPC because no supplemental mild reinforcing should be required. If the optimized shape of the UHPC girder can be proven and standardized and becomes more commonly used, the price of a UHPC bridge should become competitive with that of an ordinary HPC prestressed girder bridge with a cast-in-place deck.

The benefits of a bridge constructed with the UHPC optimized girders should be the long-term durability, due to the low permeability of the UHPC, and rapid construction. The optimized double-tees can be set adjacent to each other, connected with a simple closure pour, and then an asphalt overlay can be placed. The construction time for this type of bridge should be much less than for a bridge with a cast-in-place deck.

RECOMMENDATIONS FOR FURTHER RESEARCH

- Further verification of the proposed equation for the prediction of punching shear capacity of UHPC slabs should be performed. The specimen sample was limited and only a few parameters were varied; more data would aid in validating the model.

- Additional testing on UHPC slab specimens should be performed with variations in the following parameters:

  —slab thickness
  —slab aspect ratio
  —compressive strength

—tensile strength
—fiber volume
—loading plate area
—loading plate aspect ratio
—restraint conditions
—loading rate effects
—dynamic effects
—contribution of tensile reinforcement
—effects of in-plane forces on punching shear strength.

- Tests should be performed to determine flexural strength of the slabs in the primary direction of fiber orientation and perpendicular to the fiber orientation. It is assumed that the flexural strength in the two directions is different, and this difference will influence the prediction of flexural strength of UHPC slabs.

REFERENCES

AFGC Scientific and Technical Documents. *Ultra High Performance Fibre-Reinforced Concretes – Interim Recommendations.* (Documents scientifiques et techniques – Betons fibres ultra-hautes performances – Recommandations provisoires), French Association of Civil Engineering (Association Francaise de Genie Civil), 2002.

ASCE-ACI Task Committee 426. The Shear Strength of Reinforced Concrete Members. *ASCE – Journal of the Structural Division*, Vol. 99, No.6, 1973, pp. 1091-1187.

ASCE-ACI Task Committee 426. The Shear Strength of Reinforced Concrete Members-Slabs. *ASCE – Journal of the Structural Division*, Vol. 100, No. 8, 1974, pp. 1543-1591.

ACI Committee 318. *Building Code Requirements for Structural Concrete, ACI 318-02, and Commentary, ACI 318R-02*. American Concrete Institute, Farmington Hills, MI, 2002.

Ahlborn, T, Steinberg, E.P., Hartmann, J.L., Graybeal, B.A., Potter, J.L., and Volygi, J. Ultra-High Performance Concrete – Study Tour 2002. *Proceedings of the 2003 International Symposium on High Performance Concrete,* on CD, Orlando, FL, 2003.

Bonneau, O., Poulin, C., Dugat, J., Richard, P., and Aitcin, P-C. Reactive Powder Concretes: From Theory to Practice. *Concrete International,* Vol. 18, No.4, 1996, pp. 47-49.

Cousins, T.E. *Load.* CEE 5484 – Advanced Bridge Design Course Presentation, Virginia Polytechnic Institute and State University.

Fuchs, W., Eligenhausen, R., Breen, J.E. Concrete Capacity Design (CCD) Approach for Fastening to Concrete. *ACI Structural Journal*, Vol. 92, No.1, 1995, pp. 73-94.

Graybeal, B.A., Hartmann, J.L. Strength and Durability of Ultra-High Performance Concrete. *Proceedings of the 2003 PCI National Bridge Conference*, (on CD) 2003.

Graybeal, B.A. E-mail communication, August, 2004.

Keenan, W.A. *Strength and Behavior of Restrained Reinforced Concrete Slabs Under Static and Dynamic Loadings*. Technical Report R 621. Naval Civil Engineering Laboratory, Port Huenueme, CA, 1969.

Lafarge North America Inc., accessed September 7, 2004. Ductal's Durability Properties. Lafarge North America Inc., Herndon, VA. Internet Address: http://www.imagineductal.com/imagineductal/home.asp

Narayanan, R., Darwish, I.Y.S. Punching Shear Tests on Steel Fibre Reinforced Micro-concrete Slabs. *Magazine of Concrete Research*, Vol. 39, No. 138, 1987, pp. 42-50.

Park, H., Ulm, F-J., Chuang, E. *Model-Based Optimization of Ultra High Performance Concrete Highway Bridge Girders.* CEE Report R03-01. Massachusetts Institute of Technology, Cambridge, MA, 2003.

Park, R., Gamble, W.L. *Reinforced Concrete Slabs – Second Edition.* John Wiley & Sons, Inc., New York, NY, 2000, pp. 551-620.

Perry, V.H. A Revolutionary New Material for New Solutions. Technical Forum Presentation, Lafarge North America, 2003a.

Perry, V.H., Zakariasen, D. Overview of UHPC Technology, Materials, Properties, Markets and Manufacturing. *Proceedings of the 2003 Concrete Bridge Conference*, Orlando, FL, 2003b.

Semioli, W.J. The New Concrete Technology. *Concrete International*, Vol. 23, No. 11, 2001, pp. 75-79.

Shaaban, A.M., Gesund, H. Punching Shear Strength of Steel Fiber Reinforced Concrete Flat Plates. *ACI Structural Journal*, Vol. 91, No.3, 1994, pp. 406-414.

Tan, K.-W., Paramasivam, P. Punching Shear Strength of Steel Fiber Reinforced Concrete Slabs. *Journal of Civil Engineering Materials*, Vol. 6, No. 2, 1994, pp. 240-253.

TFRC – Turner-Fairbank Highway Research Center, accessed November 11, 2004. "High Performance Concrete Bridge Project Fact Sheets – Virginia Avenue Over the Clinch River, Richlands", McLean, VA. Internet Address: http://www.tfhrc.gov/structur/hpc/flyers.htm

Ulm, F-J., Chuang, E. *UHPC Design Issues.* Technical Forum Presentation, Massachusetts Institute of Technology, Cambridge, MA, 2003.

Yankelevsky, D.Z., Leibowitz, O. Punching Shear in Concrete Slabs. *International Journal of Mechanical Sciences*, Vol. 41, No. 1, 1999, pp. 1-15.

APPENDIX

SUMMARY OF RESULTS

Table A1. Small Slab Test Results

Slab Thickness in	**Square Punch Size** in	**Observed 1st Cracking Deflection** in	**Observed 1st Cracking Load** kips	**Failure Load** kips	**Mechanism of Failure**
2.17	1.5	0.06	6.7	23.3	Punching Failure
2.32	2	0.05	6.1	27.2	Punching Failure
2.12	1	no data	8.0	22.6	Punching Failure
2.61	2	0.06	7.9	33.0	Punching Failure
2.58	3	0.08	9.9*	35.9	Flexural Failure
2.54	1.5	0.05	8.0	30.5	Punching Failure
2.76	2.5	0.06	9.1	34.2	Flexural Failure
3.10	2.5	0.05	14.9	39.0	Flexural Failure
2.83	1.5	0.11	19.8	35.2	Punching Failure
3.03	1	0.05	14.9	40.1	Punching Failure
2.85	2	0.12	15.1	38.4	Flexural Failure
3.27	1.75	0.06	13.4	39.4	Flexural Failure

- Slab was accidentally loaded prior to starting test, resulting in an initial crack (no measurements). Load indicated is when the first crack was observed after testing began.

Table A2. Large Slab Test Results

Slab Thickness in	**Punch Size** in x in	**Observed 1st Cracking Deflection** in	**Observed 1st Cracking Load** kips	**Failure Load** kips	**Mechanism of Failure**
3.05	8 x 20	0.08	9.5	27.9	Flexure
2.80	8 x 20	0.08	8.5	22.9	Flexure
2.70	8 x 20	0.10	6.3	14.7	Flexure